

132 M-WASH D.C

RECEIVED

NEG C

ANNUAL REPORT

RESEARCH UNIT: 140
REPORTING PERIOD: 4/1/76 - 3/31/77
PRINCIPAL INVESTIGATOR: JERRY GALT

Prepared by J. A. Galt, J. E. Overland, C. S. Smyth, Y. J. Han, C. H. Pease

SECTION I. INTRODUCTION

The following report is a synopsis of modeling efforts in support of OCSEAP work around Alaska. Included are program development for an advanced spill model for use anywhere along the Alaskan coast, diagnostic model studies of ocean surface currents around Kodiak, advection trajectory model studies in the Gulf of Alaska, a coastal marine meteorology model applied along the southeast Alaskan coast, a study of the circulation of the Bering Sea, and a report on the status of computer hardware and software in support of the modeling efforts. The proponents of the various developments" pieces are as follows:

1. Advanced Model - Gait, Karpen
2. Trajectory Model - Gait, Pease
3. Diagnostic Model - Gait, Watabayashi
4. Meteorological Model - Overland, Gait
5. Bering Sea Model - Han, Gait
6. Status of Computer - Smyth, Gait

The basic framework of the advanced oil spill model has been completed. The program control modules are being tested interactively on the PDP11/34. Additional advanced model development is awaiting the implementation of an additional 32K words of memory and 2m byte disk capacity to the operating system. Documentation in the form of a programmers and users manual is being written describing the special features of the overall model and the available algorithms.

The advanced model will incorporate each of the environmental models mentioned above and reference and mesh the output from each piece into a cohesive package. For example, the advanced spill model will take the results of the diagnostic model for a given region and the regional meteorological model over the same area and combine them through the techniques developed to predict advection and dispersion in the simple trajectory model.

The creation of the data base for these studies has been largely dependent on the help of other OCS investigators. Dr. Andy Bakun supplied wind data from FNWC for the simple trajectory model project. Dr. Tom Royer of the University of Alaska gave physical oceanographic data around Kodiak for use, in the trajectory model. Mr. Bob Charney supplied current meter data for the Gulf of Alaska. Dr. Stan Hayes offered sea surface elevation specifications for the diagnostic model. Dr. Jim Schumacher discussed current meter data in the Gulf of Alaska. Mr. Mike Reynolds supplied topographic information and initial verification winds for the regional meteorological model tests in exchange for a working copy of the model. And Dr. Felix Favorite of NMFS collected physical oceanographic station data used in the diagnostic model studies.

The following report includes preliminary results from several of the developmental models. These results represent only initial explorations into the current and wind conditions along the Alaskan continental shelf and are not final model predictions.

SECTION II. DIAGNOSTIC MODEL STUDY AROUND KODIAK

The diagnostic model developed at PMEL has been used to study the Kodiak Island region as part of the OCSEAP research. In this study a number of improvements have been incorporated into the model which make the model run more efficiently, clear up certain ambiguities related to the specification of boundary conditions and improve the graphics presentation. These recent developments are being documented in two technical reports in preparation (Watabayashi, 1977 and Watabayashi and Gait, 1977).

The diagnostic model was run using two separate sets of density data. The first set of stations were collected in April and May, 1972 (Favorite, et al, 1975) and were used as a preliminary check of the regional response to be expected from the model. Although not collected specifically for input to a model, these stations gave good coverage of the region of interest, made it possible to obtain a preliminary look at the currents, and experiment with various specifications of the open ocean boundary conditions. One difficulty with this data set, however, was that the station locations did not specifically resolve some of the complex bathymetry associated with the banks off shore from Kodiak. The second set of density data used for the study was collected in April, 1976 on the OCSEAP sponsored Moana Wave Cruise with Dr. T. Royer Chief Scientist. In this case the data was specifically stationed to resolve the bathymetry. This second set of data was used for most of the investigations reported below.

The use of the diagnostic model on the Kodiak region was different from previous studies in three specific ways that relate to the formulation of the boundary conditions and forcing functions. As before, the offshore sea surface elevation in deep water was determined by assuming a level of no motion at 1000 to 1200 meters and along solid boundaries or coastlines, the sea surface elevation was assumed to be constant. Along open boundaries across the shelf a new procedure was carried out in two steps. First, the cross shelf sea surface slope was assumed to be proportional to the on shore component of the Ekman transport and inversely proportional to the depth, i.e.,

$$\frac{\partial \xi}{\partial \eta} \propto \frac{\tau_s}{H}$$

where η is taken as a direction normal to an isobath and s is a direction parallel to the isobath. With these values as a starting point, a reduced form of the model (ignoring the effects of bottom friction) solves the resulting first order equations to indicate which boundary values are strongly coupled. During this second stage, the coupled boundary values are adjusted in a dynamically consistent manner that guarantees a continuity balance and eliminates the extraneous lateral boundary layers that were possible in some of the previous cases and which required numerical experimentation to correct. The third modification to the program was to vary the strength of the wind stress and subsequent surface Ekman mode for consistency with the sea surface slope condition.

Wind and current meter data for the Kodiak area was very limited. At the time of the model experiments, one current meter mooring WGC-2C

(Charnell) was used along with wind data from FNWC (Bakun). The current meter mooring was positioned on the 200 meter contour just on the inner edge of the Alaskan Stream and showed consistently strong flow to the SW along the isobath. The model was able to reproduce this flow fairly well, but since the currents in this region were dominated by the deep water baroclinic Alaska Stream, they were not significantly affected by variations in the boundary condition settings. Thus, this current meter was not particularly useful for exploring variations in the flow. The wind data corresponding to the April-May, 76 period obtained from the FNWC pressure analysis showed a somewhat different set of characteristics than we obtained from the Summer/Winter analysis of the NEGOA area (ref. last year's annual report). The mean winds were small relative to the variations associated with the storm events. The record was clearly dominated by the passage of cyclones where the wind direction reversed. Because of the reversals, no attempt was made to run the model with mean wind values. Instead, a series of test winds were created that could be used for the initial model studies.

Four cases were considered, each with a uniform wind stress blowing along the SW-NE axis (parallel to the coastline]. This configuration corresponded to various degrees of Ekman transport normal to the coast (upwelling/downwelling) and was associated with the coastal barotropic set-up through the boundary conditions. The cases run were 4, 2, 1 and -1 dynes/cm² towards the SW. Assuming a quadratic stress law and typical values for the drag coefficient, this allows a maximum wind case of approximately 30 kts. (mean wind). The model output for

these cases presents surface currents (figures 1 - 4) bottom currents (figures 5- 8), and sea surface elevation (2, 1, -1 dynes/cm² cases included (figures 9 - 11).

From the preliminary results a number of tentative conclusions can be reached. These lead to the following qualified description of the regional flow.

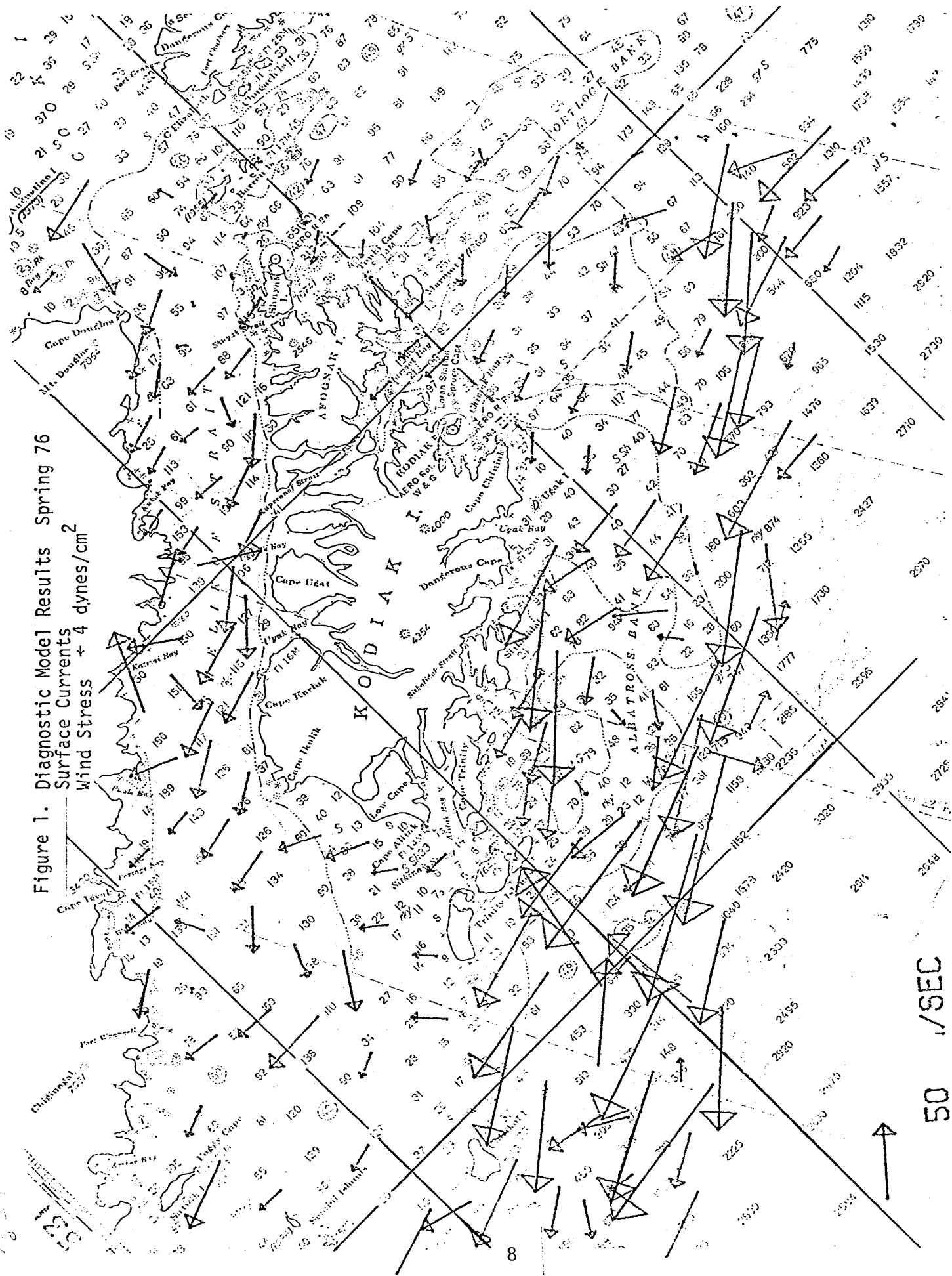
Along the edge of the continental shelf the flow is dominated by the Alaskan Stream. Here the flow is relatively narrow with a maximum magnitude of approximately two knots. This is clearly an extension of the Stream that exists along the entire northern part of the Gulf of Alaska. It has been previously described by Favorite, et al, (1975) based on the April-May 1972 data from the RV Kelez cruise. By way of review, the Stream appears to intensify toward the west or, more accurately, toward the southwest as it flows down the Aleutian Chain. One of the features of the stream suggested by the '72 data and predicted by the model using both '72 and '76 data is a broadening of the Alaskan Stream just SW of the Trinity Islands. This appears to be associated with the bathymetry just downstream from Albatross Bank where a shoal is separated from the main section of the Bank by a deeper channel. The effects of variations in the wind stress have a minimal effect on the flow within the Alaskan Stream. This is built into the model through the boundary conditions and reflects our fundamental belief that this current is baroclinically controlled by processes with time scales that are long compared to local variations in the wind forcing.

The continental shelf SE of Kodiak can be characterized by a series of banks separated by channels that provide deeper access to the waters crossing the shelf. Starting with Portlock Bank, this bank and channel pattern repeats itself with Marmot Bank and then Albatross Bank, which is itself cut in two by a channel off shore from Sitkalidak Island. Beyond Albatross Bank the 100 fa. contour again cuts in towards shore south of the Trinity Islands. Based on these preliminary model studies, it appears that these deeper channels crossing the shelf have a significant roll in the regional circulation. Under the influence of winds towards the SW (figures 1 - 3), these deeper channels tend to have onshore flow. The effect is particularly pronounced south of Portlock Bank and off Sitkalidak Island. In both these cases, the cross shelf channels lead into deeper regions oriented parallel to the coastline and the flow can continue as a coastal current. The channel SW of Marmot Bank does not appear to develop the onshore flow using the '76 data. With the '72 data this region developed weak onshore flow. But with limited access to deeper regions inshore, simple continuity arguments suggest this channel will not develop as vigorous an onshore flow and consequently, not contribute in a major way to the exchange of nearshore waters with the waters of the outer continental shelf. Under the influence of weak winds towards the NE (figure 4), the flow through these channels is not obvious, although the channel off shore from Sitkalidak Island appears to have flow inshore on the SW side and off shore on the NE side. Having studied only one case, these results must be considered as little more than indicative of possible flow patterns. A more realis-

Figure 1. Diagnostic Model Results Spring 76

Surface Currents

Wind Stress ± 4 dynes/cm²



50 /SEC

tic appraisal of the NE wind stress case will have to wait for better observational data and additional model tests.

One of the more interesting circulation features suggested by the present model studies is the coastal current. This is particularly well-developed along the south side of Kodiak between Dangerous Cape and Cape Trinity. For the case with strong wind to the SW, (figure 1), this flow obtains speeds of nearly two knots and is thus comparable in magnitude to the Alaskan Stream. As mentioned previously, this area has a relatively deep nearshore channel running inside the bank. In addition, this area has relatively free communication with the outer continental shelf via the channel through Albatross Bank. This current then appears to be caused by the barotropic set-up along the coast plus the extension of the onshore flow from this channel. With decreased winds toward the SW, the magnitude of this current drops off substantially, and the model shows speeds of a few tens of centimeters per second for a 1 dyne/cm² wind stress to the SW (figure 3). For the NE wind stress case, the direction of the coastal flow is seen to reverse with the region of strongest flow off Dangerous Cape, once again apparently associated with the channel across Albatross Bank. Without any observational data, it is difficult to evaluate how well the model is calibrated for this area. That we get current reversals for reasonable ranges of expected input parameters is interesting in itself and suggests that this area is worth more study, particularly since the actual direction of the flow may reverse and the region appears to have significant exchange of water across the shelf.

Figure 6. Diagnostic Model Results Spring 76
Bottom Currents
Wind Stress $\leftarrow 2 \text{ dynes/cm}^2$

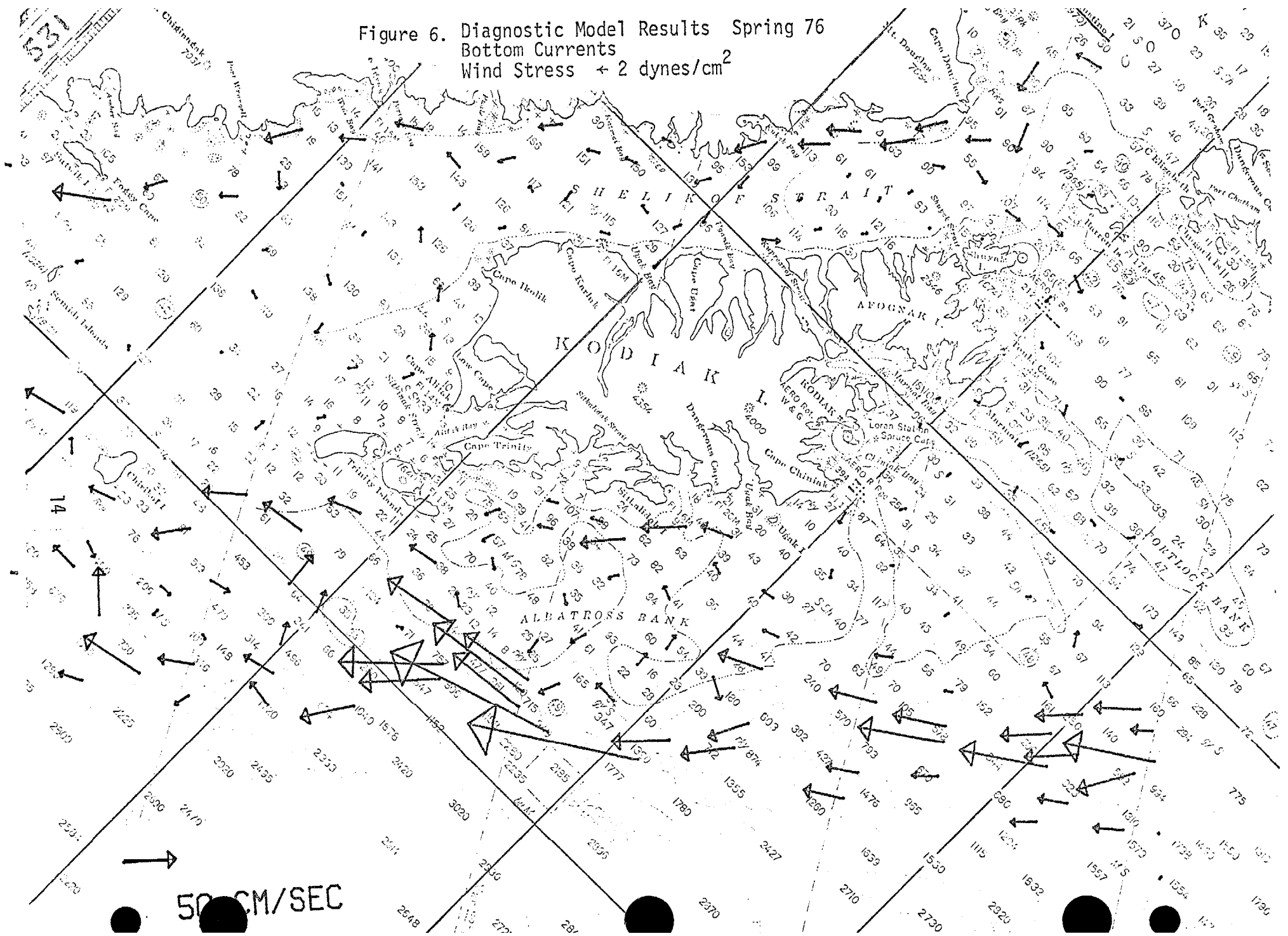
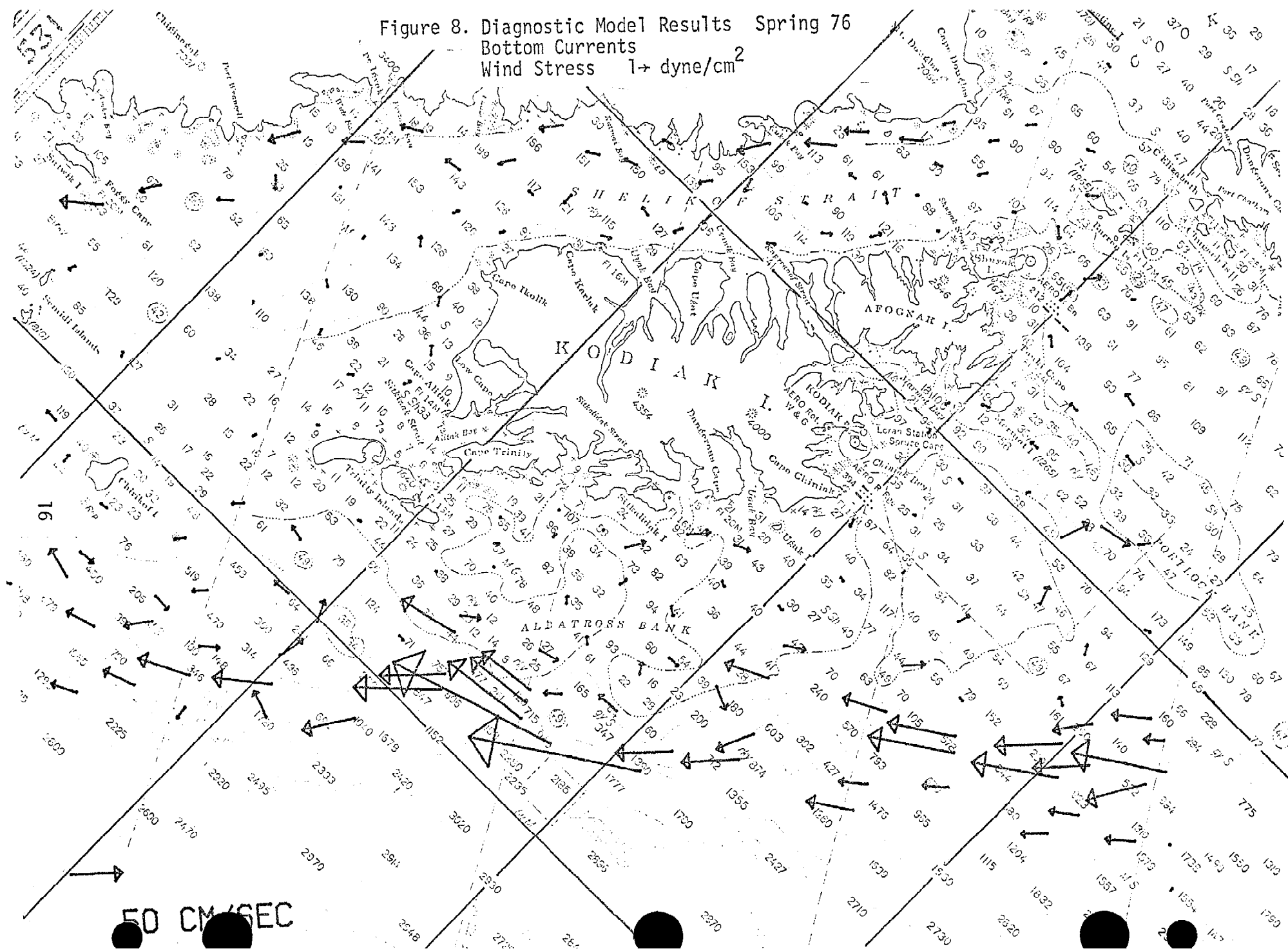


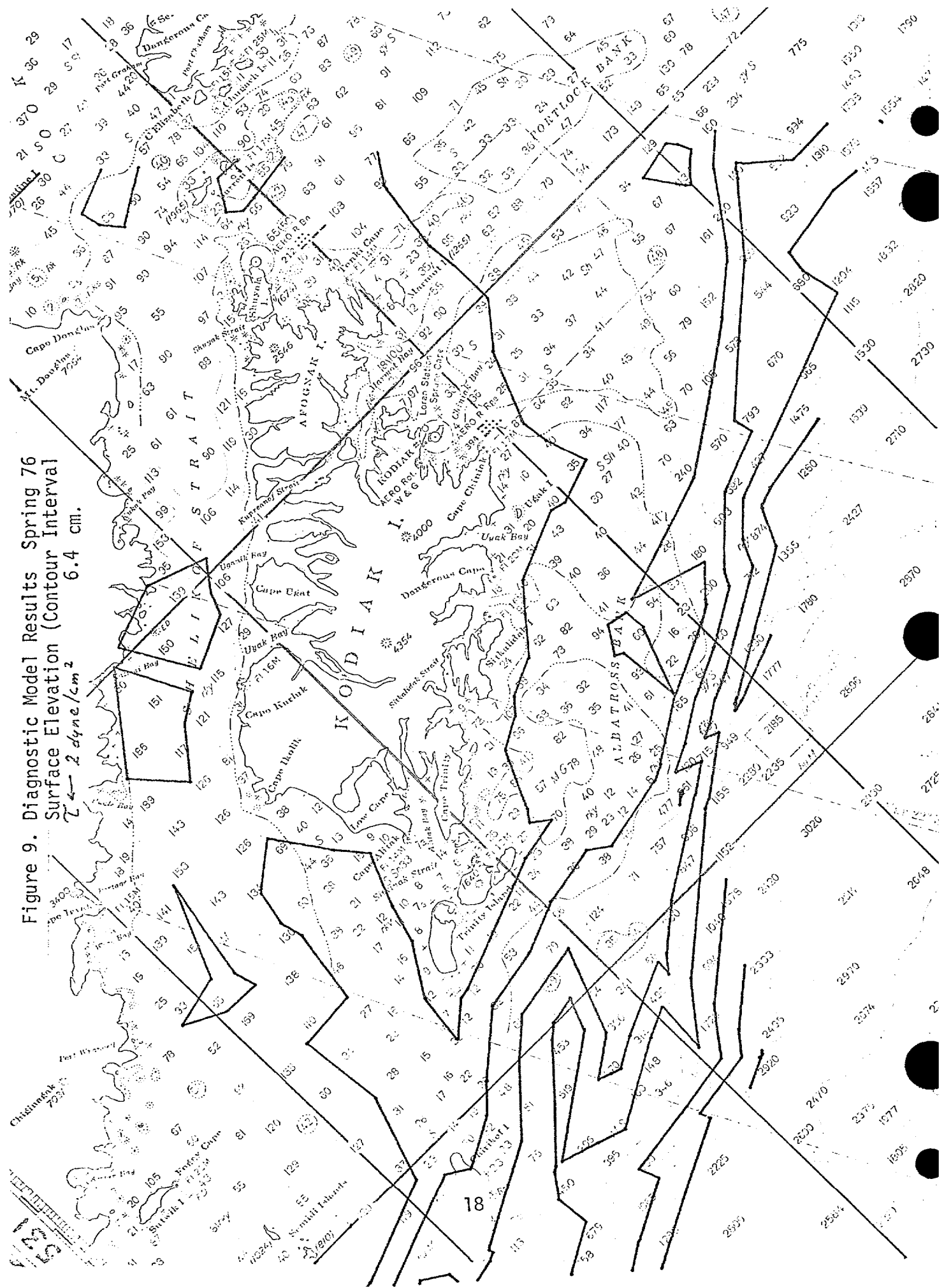
Figure 8. Diagnostic Model Results Spring 76
Bottom Currents
Wind Stress $1 \rightarrow \text{dyne/cm}^2$



The model predicts bottom currents (geostrophic flow at the bottom) as well as surface currents. These are presented in figures 5 - 8 and can be described as generally similar to the surface flow patterns except that the bottom currents magnitudes tend to be smaller and their direction tends to be slightly different to compensate for the onshore or offshore transport of the surface Ekman flow. For example, comparing figures 1 and 5 for the area off Dangerous Cape indicates that the surface flow has a slight onshore component and consequently, the bottom flow shows a component offshore. Similarly, west of Kodiak off Low Cape, the surface currents show an offshore component and the deeper flow has an onshore component. In general, the bottom currents do not show a current reversal, but there are a few exceptional areas. A careful examination of figures 1 - 8 show that this may happen south of Portlock Bank and in some of the eastern regions of Shelikof Strait.

Figures 9 - 11 show the sea surface elevation predicted by the model. These correspond to streamlines for the flow just under the surface layer. There are two general features of these figures that are of interest. First, all the cases show a significant meander in the flow south of the Trinity Islands. This pattern is clearly related to the bathymetry and results in flow to the north (towards shore) in this region. The flow then appears to circulate in a counter clockwise loop continuing on to the southwest. Secondly, there is a major change in the surface contour closest to Kodiak Island between the SW stress and the NE stress cases (figures 10 - 11). This clearly indicates the poten-

Figure 9. Diagnostic Model Results Spring 76
Surface Elevation (Contour Interval
 2 dyne/cm^2) 6.4 cm.



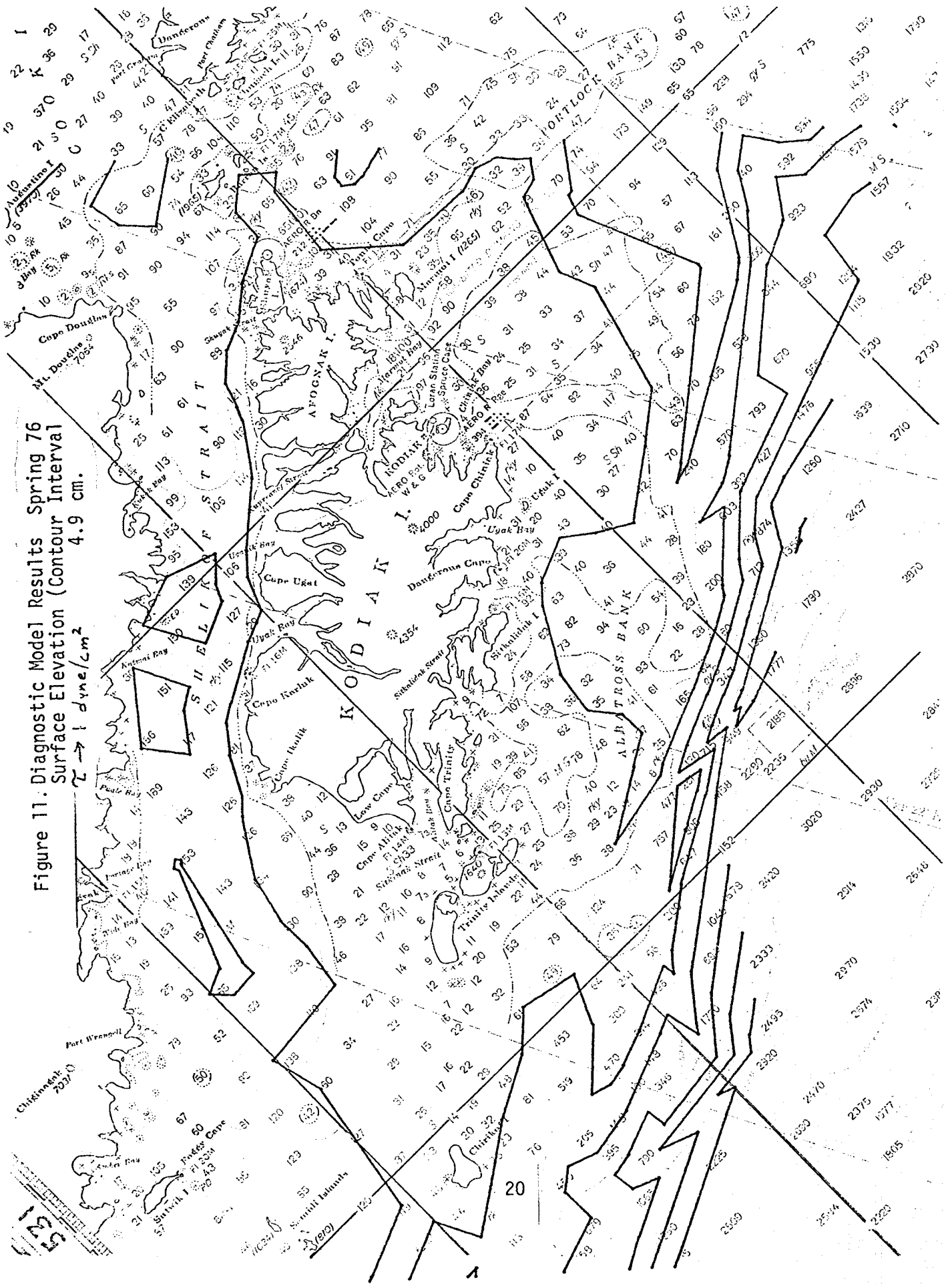


Figure 11. Diagnostic Model Results Spring 76
 Surface Elevation (Contour Interval 4.9 cm.)
 $\vec{C} \rightarrow 1 \text{ dyne/cm}^2$

1:25,000

20

54

for reversing the direction of the coastal currents around Kodiak.

From these initial studies with the diagnostic model of the Kodiak area, a number of flow characteristics have been tentatively identified which allow speculation about the regional current dynamics. It should once again be emphasized that these studies have been made with essentially no current meter verification or wind field information. These represent only a first look with the model and subsequent studies should make it possible to strengthen or discard many of these conclusions. Future plans for applying the diagnostic model in the Kodiak region call for: 1) a recommendation for the inshore placement of current meter moorings to document flow conditions in the channels and over the banks, 2) running the model for additional stress fields, in particular investigating NW and SE stress cases, as well as more intense NE stress cases, 3) running the model with a mixed boundary value formulation to better resolve coastal currents and multiply connected domains, 4) keying the model to real time wind estimates and simulate time dependent trajectories for the region, and 5) analyzing observational data to establish the proportionality coefficient relating the sea surface slope to the wind stress.

Liaison with the Kodiak physical oceanographic components of the OCSEAP study will continue with primary communication carried out by personnel exchange with the appropriate PI's. Thus far the modeling results reported here have been presented, in part, at the OCSEAP Physical Oceanographers' Review Meeting (Lake Quinalt - Oct. '76) and the

Kodiak Lease Area Synthesis Meeting (Anchorage - March '77). In addition, USGS personnel (Smyth) working on OCS assessment modeling will be advised of the status of the Kodiak studies (April '77).

SECTION III. TRAJECTORY MODEL STUDIES IN THE GULF OF ALASKA

The purpose of the preliminary trajectory model study is to investigate the possible formulations for an **advective-diffusion** model for the prediction of the movement of pollutant spills. We must legitimately ascertain if the various methods and options make any difference for prediction purposes. Such options should include trajectories based on real-time current meters and wind information with appropriate Ekman dynamics and those based on stochastic interpretations of ensemble data for the particular region of study.

The preliminary pollutant trajectory model has been written and tested with various input parameters for the Gulf of Alaska. The program allows the user to choose options of the type of physical processes to be studied. With these choices and the appropriate data inputs, the program is automatic for a given area of study. The program output is a data file or tape of trajectory positions and integer characters for the labelling of each new trajectory sequence. This data file or tape can then be read into an automatic machine-specific plot routine which will superimpose the trajectory information on a section of scaled coastline.

The component processes which can be used to run the trajectory model are: 1.) real-time currents using NEGOA current meter data for the region keyed to the results of the diagnostic model, 2.) mean currents of the same current meter data, also keyed to the results of the diagnostic model, 3.) mean plus stochastic currents based on

a Markov analysis of the same current meter record, 4.) real-time winds using six hour FNWC data for the region over the same time period as the current meter in the previous options, and 5.) mean plus stochastic winds based on a Markov analysis of the same wind record.

Figures 1 thru 6 show the results of the test cases of the model for the summer of 1974. Each trajectory on a plot runs for thirty days and they are initialized consecutively one day apart. The trajectory time step is every six hours, while the plots only give their location at the end of each week. The plotting routine also has the capability of tracing each individual trajectory with a line, but that was not implemented here since the runs were made with 50 different trajectories. The plotting package also has the capability of being used as a scatter diagram, showing a continuous cloud of points representing an overall view of the entire field of trajectory locations. This last feature would be most useful with a probability study.

Figure 1 shows the first case with a real-time ocean current and no wind. Similarly, The second case represented in figure 2 was run with a real-time current and a real-time wind. These two cases are very similar since the winds were light during the study period, except for the first few days. These results were reported earlier at NEGQA Synthesis Meeting in Anchorage.

V = VT

25

GULF OF ALASKA TRAJECTORY PLOT

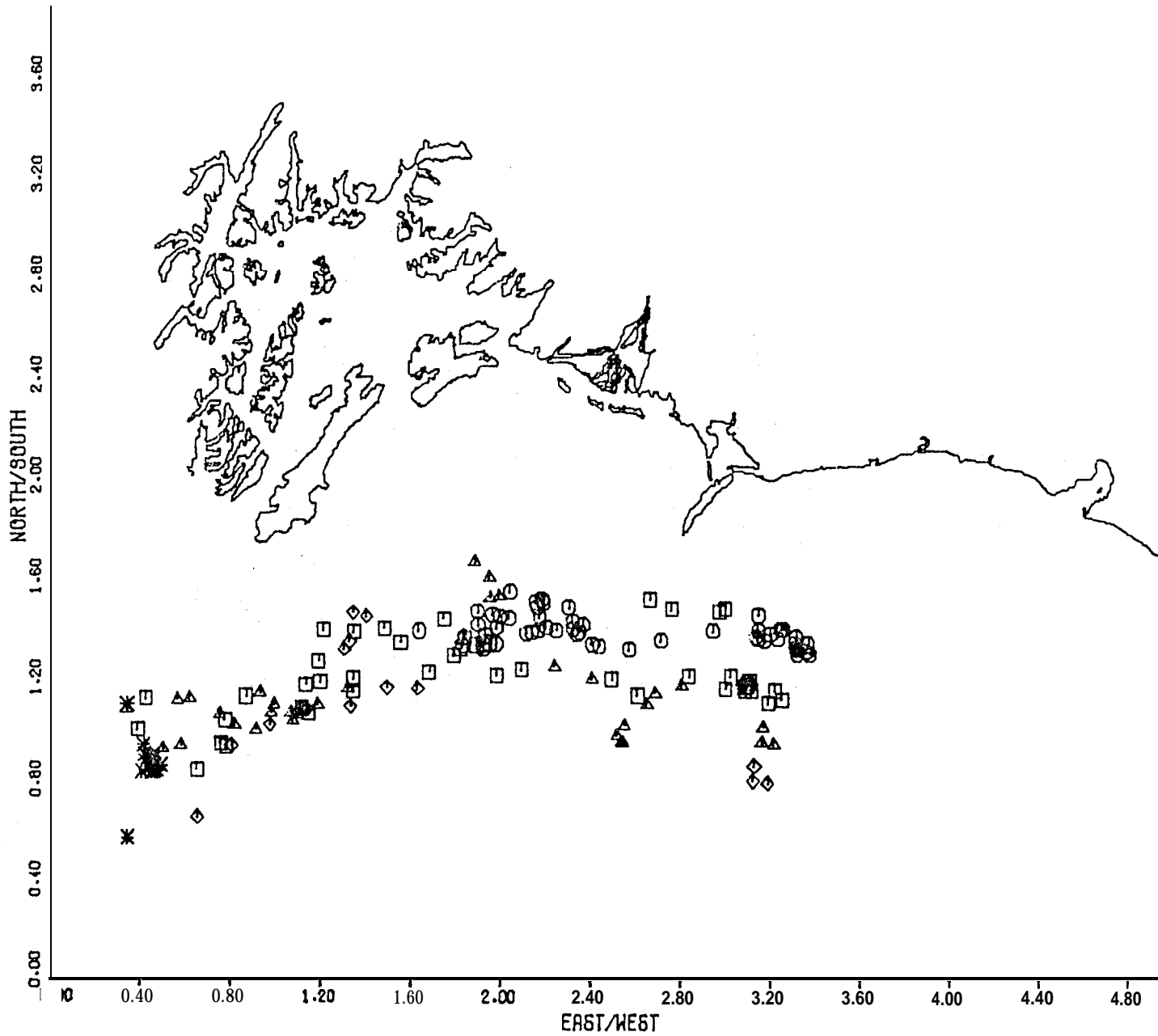


Figure 1. Trajectories based on real-time ocean currents only for summer 1974 in the Gulf of Alaska. Circles indicate end of first week, squares the second, triangles the third, and diamonds the fourth. Stars indicate the trajectory left the grid system before the end of the month.

$$V = VT + AE*(WT-WM) + AW*WT$$

GULF OF ALASKA TRAJECTORY PLOT

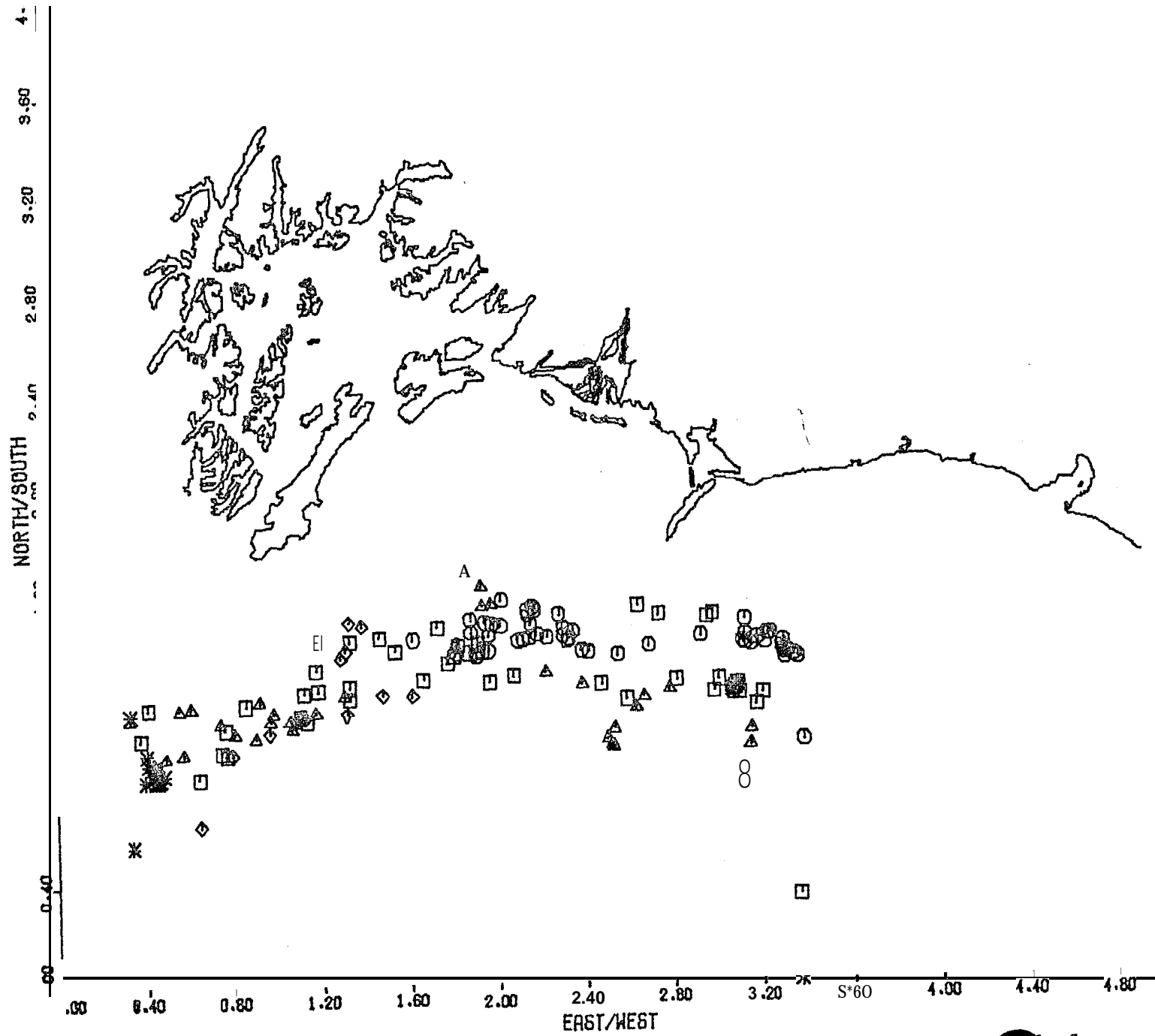


Fig. 2. Trajectories based on the real-time wind information for summer 1974 in the Gulf of Alaska. Symbols same as in Figure 1.

Figure 3 through 6 represent the results of cases using different stochastic formulations. The case shown in Figure 3 is based on a mean ocean velocity system plus a stochastic spreading component to the velocity. This case has no explicit wind formulation. Compared to the real-time results, the scatter is much greater while the bulk of the flow has a similar orientation toward the south or southwest. Figure 4 shows a case with a mean ocean system, but no ocean stochastic component. In addition, a downwind fraction of the mean wind and the stochastic wind are included. Compared to the three previous cases, the orientation of the predicted trajectories is markedly more towards the west and northwest for this fourth test. Figure 5 estimates the trajectories using the same set-up as that for Figure 4, except that an Ekman fraction of the stochastic wind is added in. This gives results more similar to those in the third case, with a large scatter, but a bulk orientation towards the south and southwest. Both case 3 and case 5 indicate several of the trajectories also beached east of Kayak Island and west along Montague Island. The last case is represented in Figure 6. This includes all the parts of the fifth case plus a stochastic ocean current component. The east/west scatter is similar to that for cases 3 and 5, but a much larger fraction of the trajectories beached to the north.

Preliminary initial results suggest that if you want to study specific events related to a pollutant spill that you will need information about the local conditions and time scale. It appears that the

$$V = VM + VS$$

GULF OF ALASKA TRAJECTORY PLOT

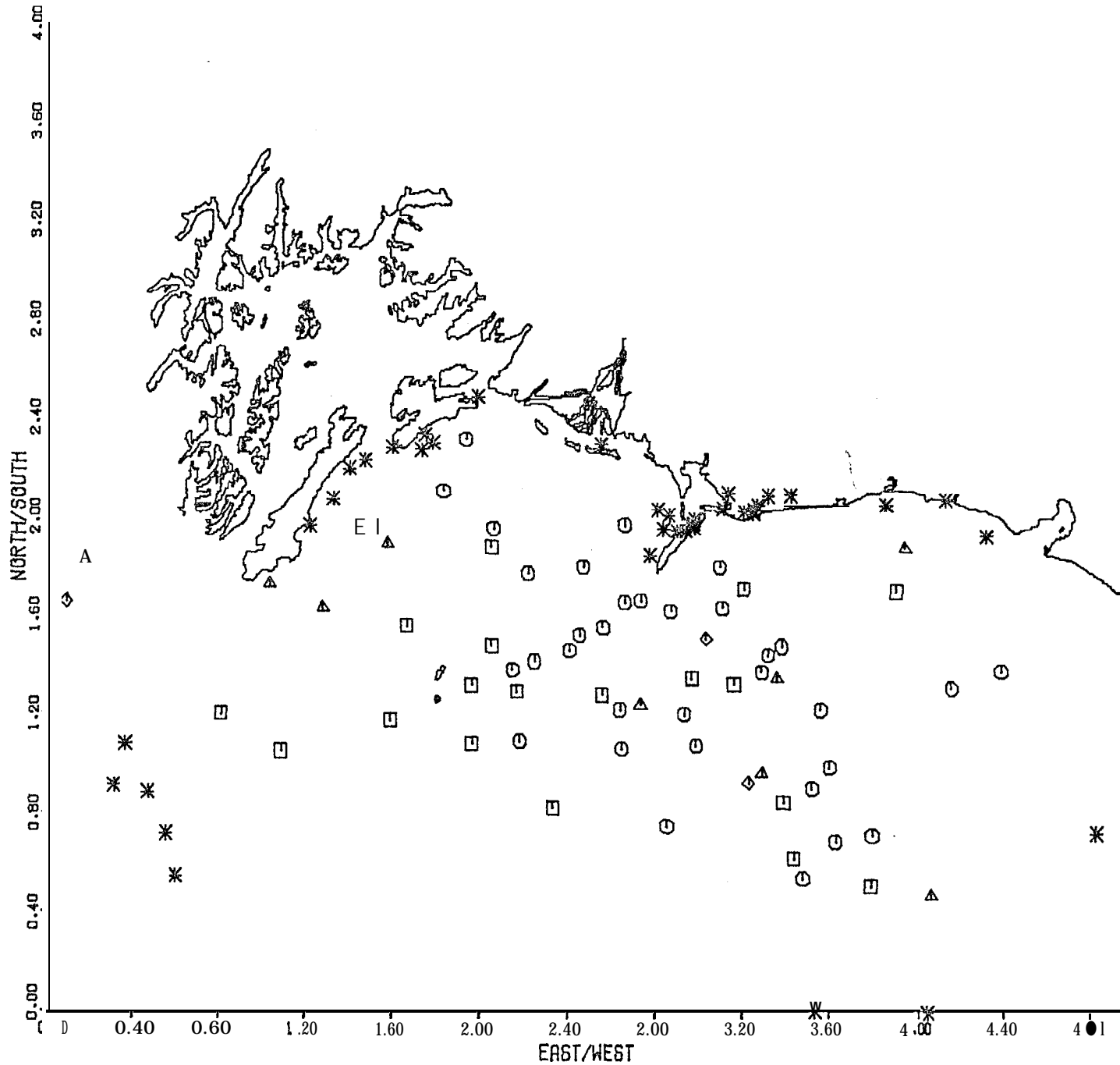


Figure 3. Trajectories based on a mean current system with stochastic spreading for summer 1974 in the Gulf of Alaska. Symbols are the same as in Figure 1.

$$V = VM + AW*(WM+WS)$$

GULF OF ALASKA TRAJECTORY PLOT

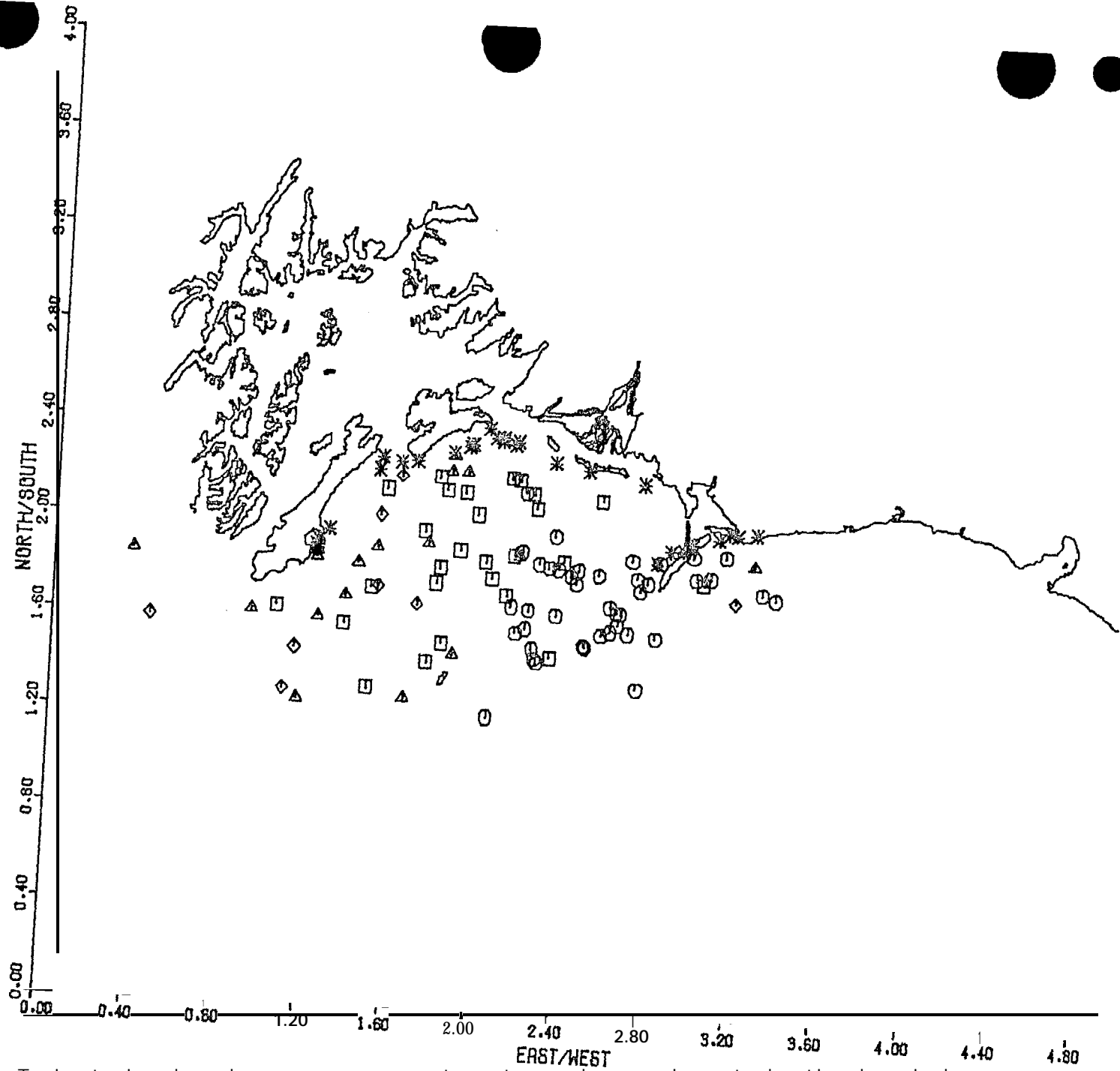


Figure 4. Trajectories based on a mean current system and mean plus stochastic downwind information for summer 1974 in the Gulf of Alaska.

Symbols are the same as Figure ?.

$$V = VM + AE*WS + AW*(WM+WS)$$

GULF OF ALASKA TRAJECTORY PLOT

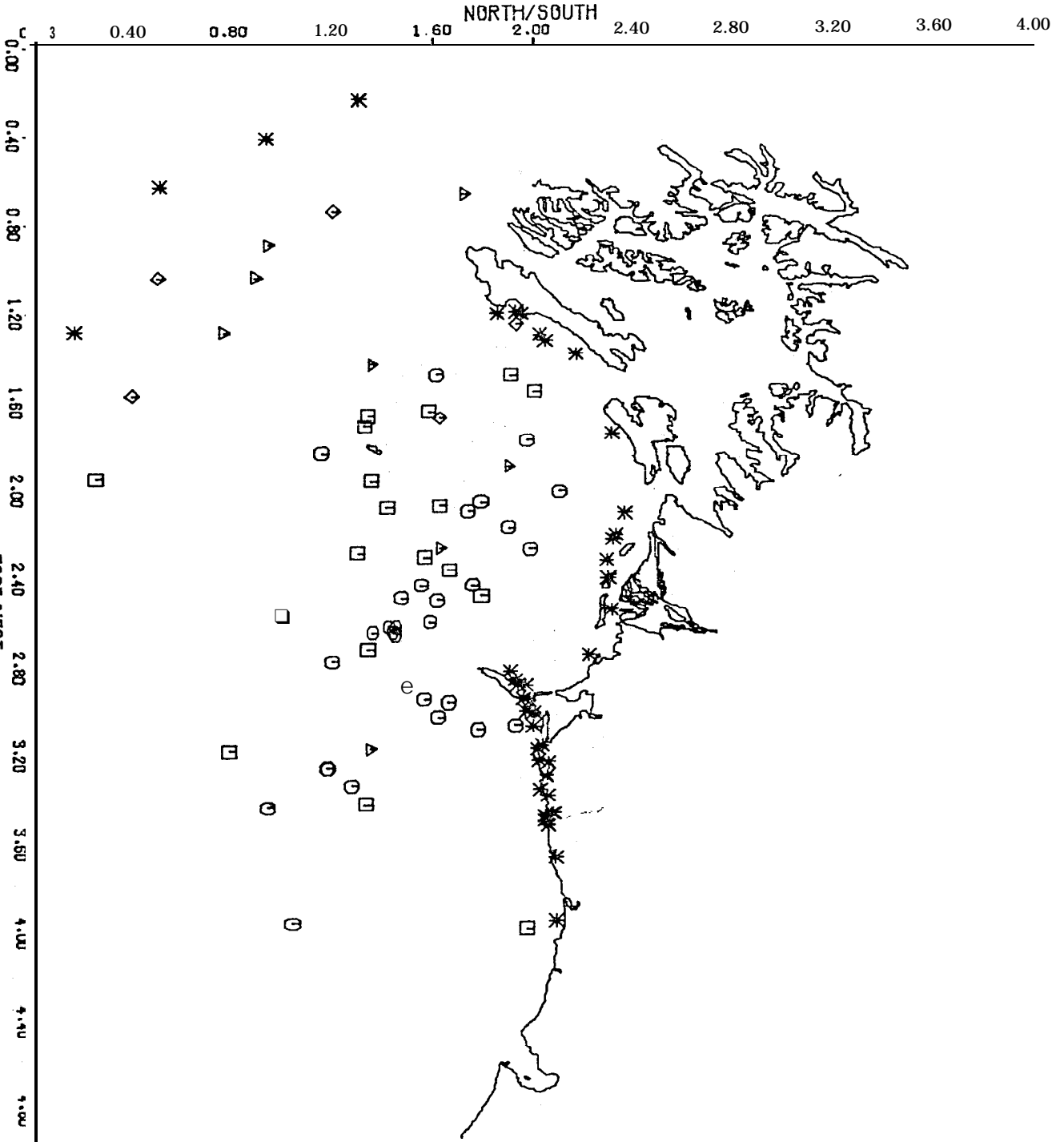


Figure 5. Trajectories based on a mean current system and mean plus stochastic downwind information and the Ekman effects of the stochastic part of the wind for summer 1961 in the Gulf of Alaska. Symbols are the same as Figure 1.

GULF OF ALASKA TRAJECTORY PLOT

$$V = VM+VS + RE*MS + RW*(M+MS)$$

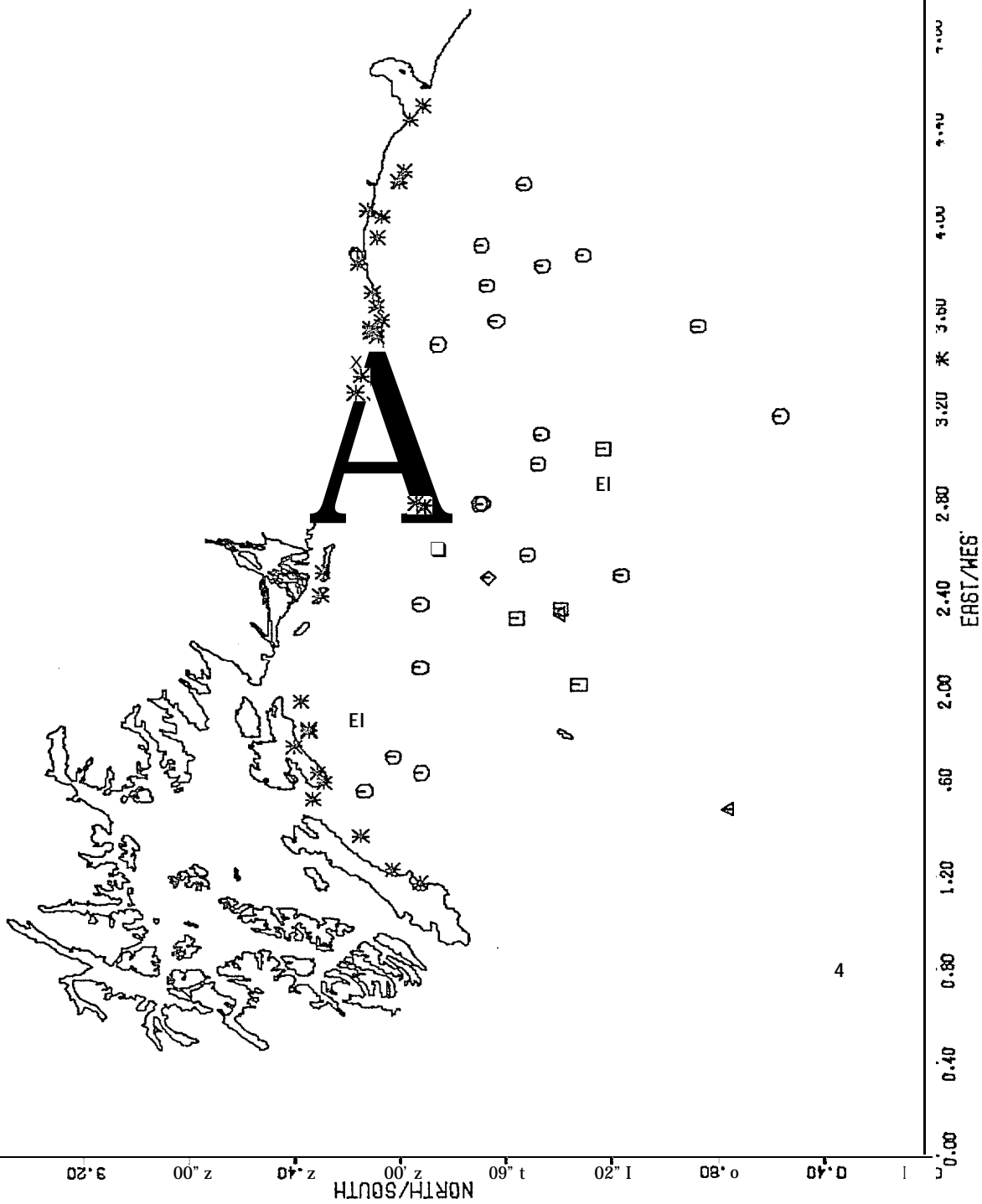


Figure 6. Trajectories based on a mean current system with stochastic spreading and mean plus stochastic downwind information and the Ekman effects of the stochastic part of the wind for summer 1974 in the Gulf of Alaska. Symbols are the same as Figure 1.

stochastic formulations give a good overview of an ensemble of possible occurrences of trajectories over a season, but do not give information related to specific events.

Another major point to be applied to an analysis of this study is that the winds and currents are not statistically independent. The major currents are Barotropic which are due to the set-up by the wind of a sea surface slope. So the correlation between the currents and the winds is not independent. This may introduce error into the cases with combined terms of wind and ocean currents. This problem makes a strong argument for the development of the independent regional meteorology model to be used in conjunction with the diagnostic model for trajectory inputs.

SECTION IV. REGIONAL METEOROLOGICAL MODEL

IV-1. Introduction

An important limitation of coastal marine meteorology is the inadequate specification of the local wind field at the desired spatial resolution. Typically, it is difficult to estimate near-shore wind fields directly from large scale synoptic patterns or scattered wind measurements because topography and discontinuities in surface roughness and heating give rise to significant mesoscale variations. For example, Fig. 1, reprinted from a NWS Technical Report to be published in early 1977, shows reported regions of anomalous wind speed and direction along the Alaskan coast. The Alaska Region of the National Weather Service compiled Fig. 1 from a survey of the Coast Guard and other groups operating vessels in Alaskan waters. Strong ageostrophic winds exist in the passes of the south-east Alaskan coast and can be attributed to channeling around islands. The open coast is also subject to anomalous winds caused by high coastal mountains. Of particular importance are Katabatic winds, forced by the contrast of warm ocean temperatures and cold temperatures 50 - 100 km inland.

This section reports on one approach to ascertaining the magnitude of mesoscale effects. A numerical model, which consists of fairly general conservation statements for mass, momentum, and heat, represents the behavior of the lower atmosphere. Within the context of its formulation, the model is used to document the implications of change in large scale flow, surface parameters, and assumed dynamics

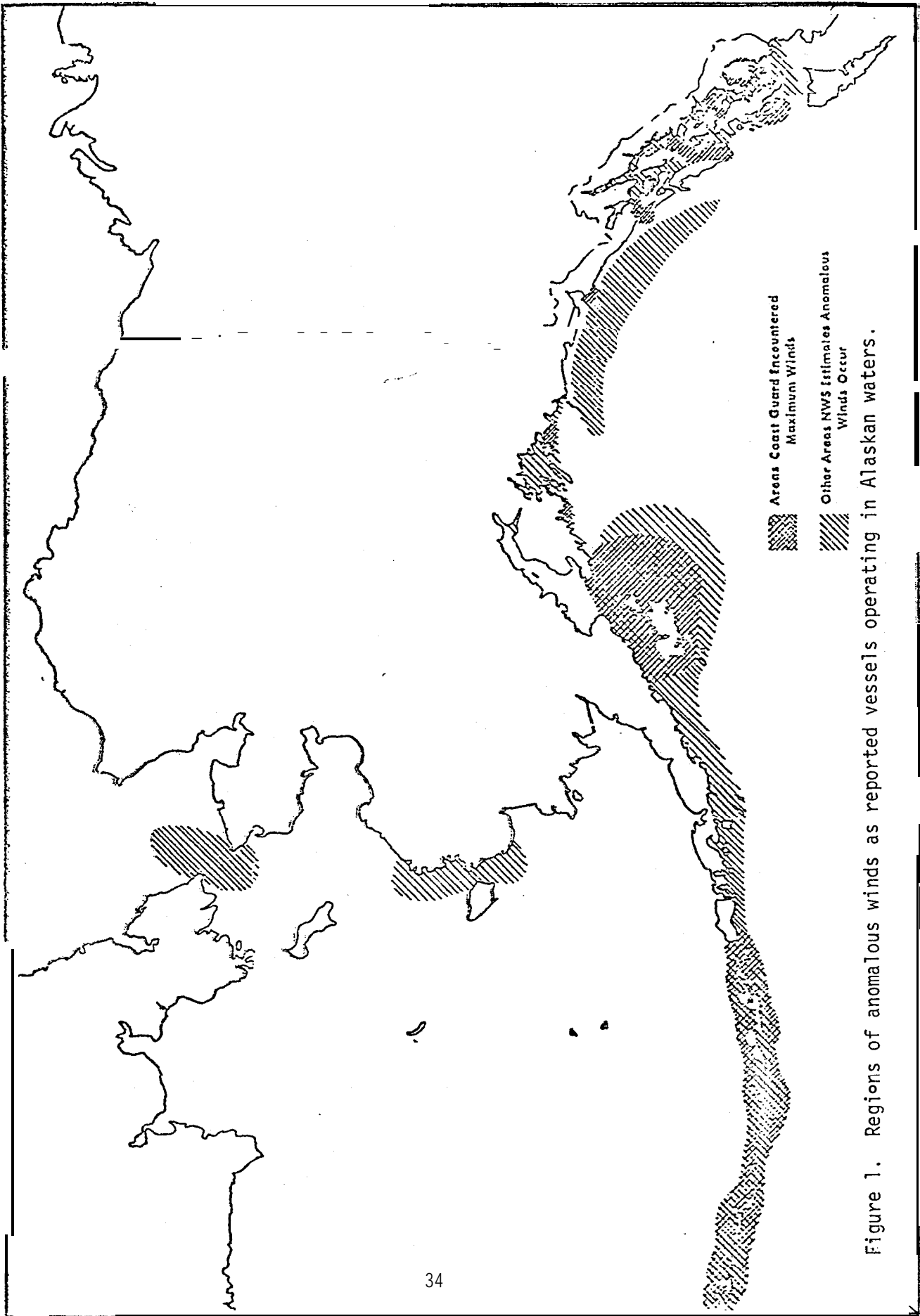


Figure 1. Regions of anomalous winds as reported vessels operating in Alaskan waters.

on the wind pattern in a limited region. A major goal is the ability to infer local winds at important maritime locations from the large scale flow pattern.

We have chosen to adapt a model proposed by Lavoie (1972, 1974). Lavoie treats the planetary boundary layer (PBL), typically 0.5 to 2 km deep, as a one layer, vertically integrated primitive equation model. The model solves for the two components of horizontal velocity, boundary layer height, and potential temperature throughout a limited region. Large scale geostrophic wind, surface elevation and temperature, and the stability of the air in the free layer above the PBL are specified as boundary conditions. Air temperature and PBL height are specified at the inflow boundaries. The local response is calculated by specifying smooth initial values of wind, temperature, and PBL height and then time stepping the equations of continuity, momentum, and heat conservation until an equilibrium state is obtained. The system is free to estimate land-water contrast, modification of the down wind environment by advection, and channeling by topography. The equilibrium state is considered to give the local winds which occur in conjunction with the given large scale pressure pattern. Since the model consists of only one layer, processes which depend upon vertical structure such as intensification of fronts cannot be directly resolved; however, the model should be well suited to estimating wind patterns in mountainous regions with strong orographic control.

A complete description of the model formulation and computer code is available as a forthcoming Technical Report. The remainder of this section discusses preliminary testing using Puget Sound as a base, and

initial application of the model along the Alaskan coastline.

lv-2. Simulation for Puget Sound - Strait of Juan de Fuca

Puget Sound was selected as location to test the suitability of the model to simulate orographic control. The principal rationale was the accessibility of a large operational data base for verification as well as an existing digitized topographic grid.

We have initially selected to simulate two generalized meteorological flow conditions for the Puget Sound System, corresponding to summer and winter regimes. In the summer months, anticyclonic flow around a well-developed semi-permanent high pressure cell to the west of the region causes prevailing northwest winds offshore along the western coasts of Washington and Vancouver Island. By midwinter the prevailing flow is southwesterly, as the region comes more under the influence of the cyclonic circulation of the Aleutian low. An important winter case, however, that we have not chosen to investigate is high pressure to the east of the region which gives easterly winds, particularly along the Strait of Juan de Fuca.

A location map for western Washington is provided in Fig. 2. Topographic data for Puget Sound was obtained from a master tape at the National Center for Atmospheric Research (NCAR). The mesh is a 5 minute of latitude by 5 minute of longitude grid with an average elevation computed for each square. The NCAR tape also specified if the square was land, ocean, part land and ocean, or part lake. The NCAR elevation data was smoothed in both directions with a 1-2-1 type smoother (Shuman, 1957). Fig. 3 presents a view of the smoothed topo-

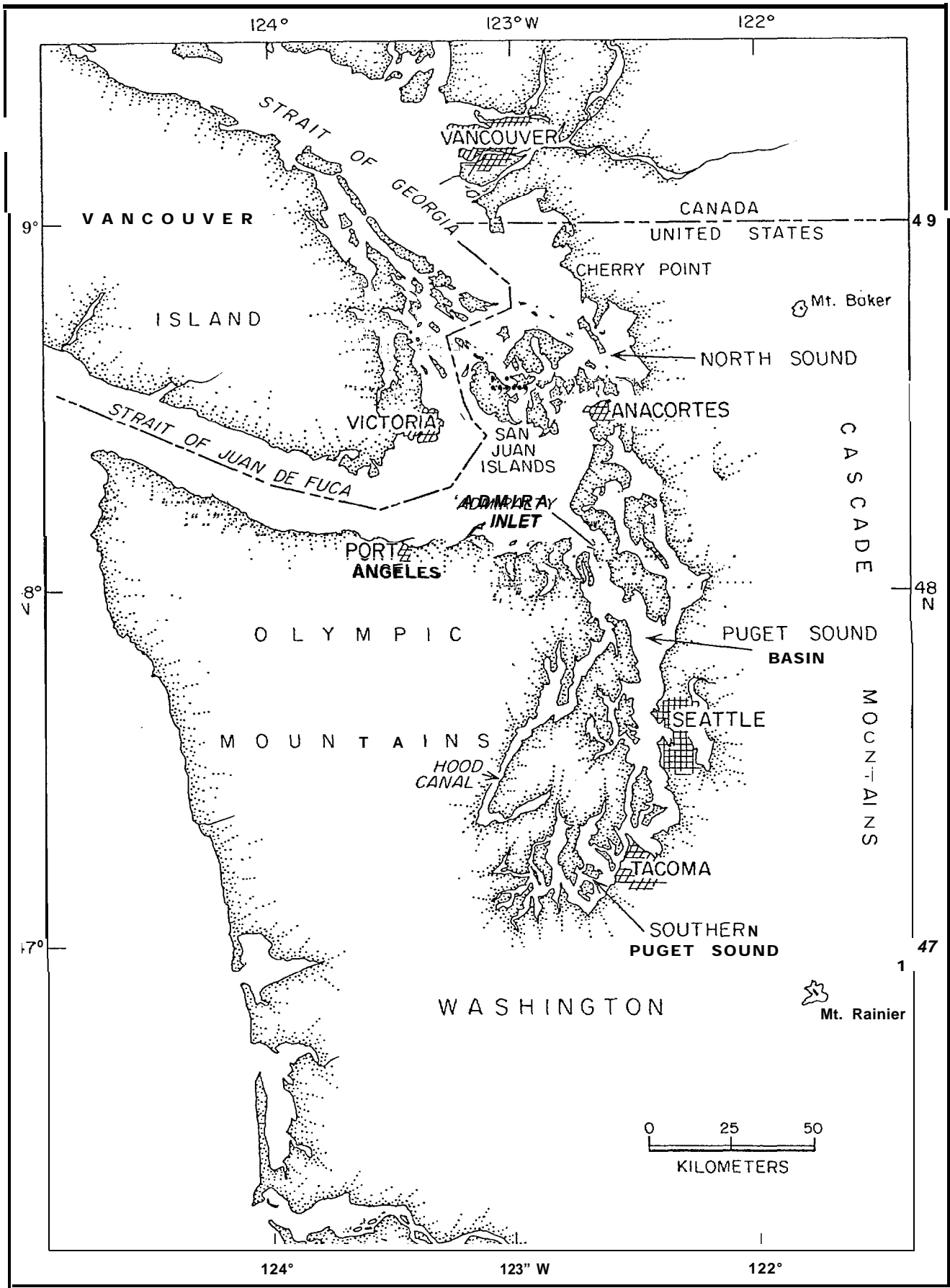


Figure 2. Location map for the Puget Sound Basin.

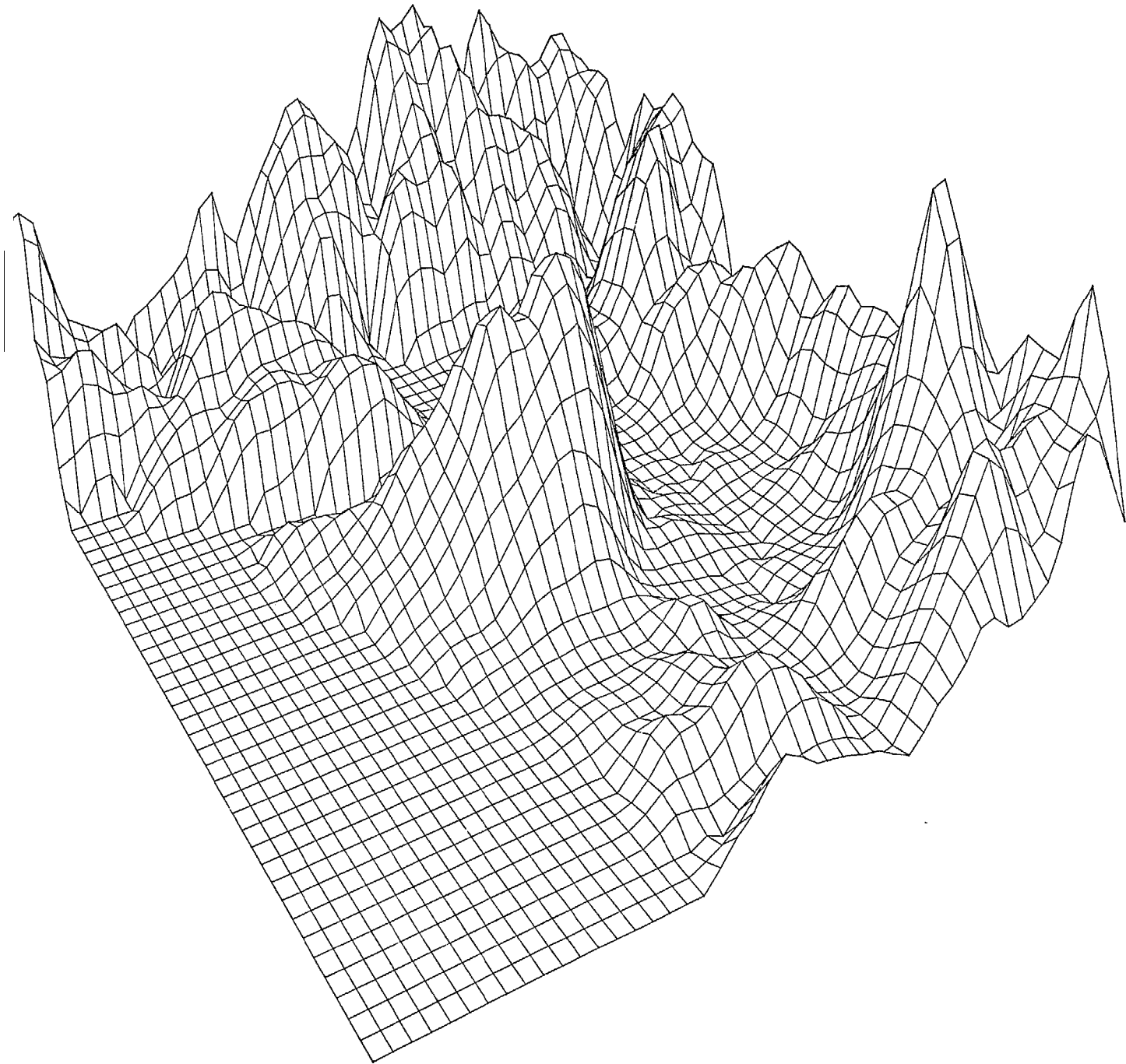


Figure 3. Topographic grid used in the computations as viewed from the southwest.

graphic grid as viewed from the southwest.

The following values of parameters and input conditions were used. They are generalized from measurements obtained during December, 1976.

$$f = 1.08 \times 10^{-5} / \text{sec}$$

$$g = 980.6 \text{ cm/sec}^2$$

$$\Delta\theta = 3.0^\circ \text{K}$$

$$o = 282^\circ \text{K}$$

$$C_D = 1.3 \times 10^{-3} \text{ (water)}$$

$$C_D = 9.0 \times 10^{-3} \text{ (land)}$$

$$C_H = 1.3 \times 10^{-3} \text{ (water)}$$

$$C_H = 7.0 \times 10^{-3} \text{ (land)}$$

$$h_i = 1.2 \text{ Km}$$

$$V_g = 10 \text{ m/s at } 245^\circ \text{ for SW flow}$$

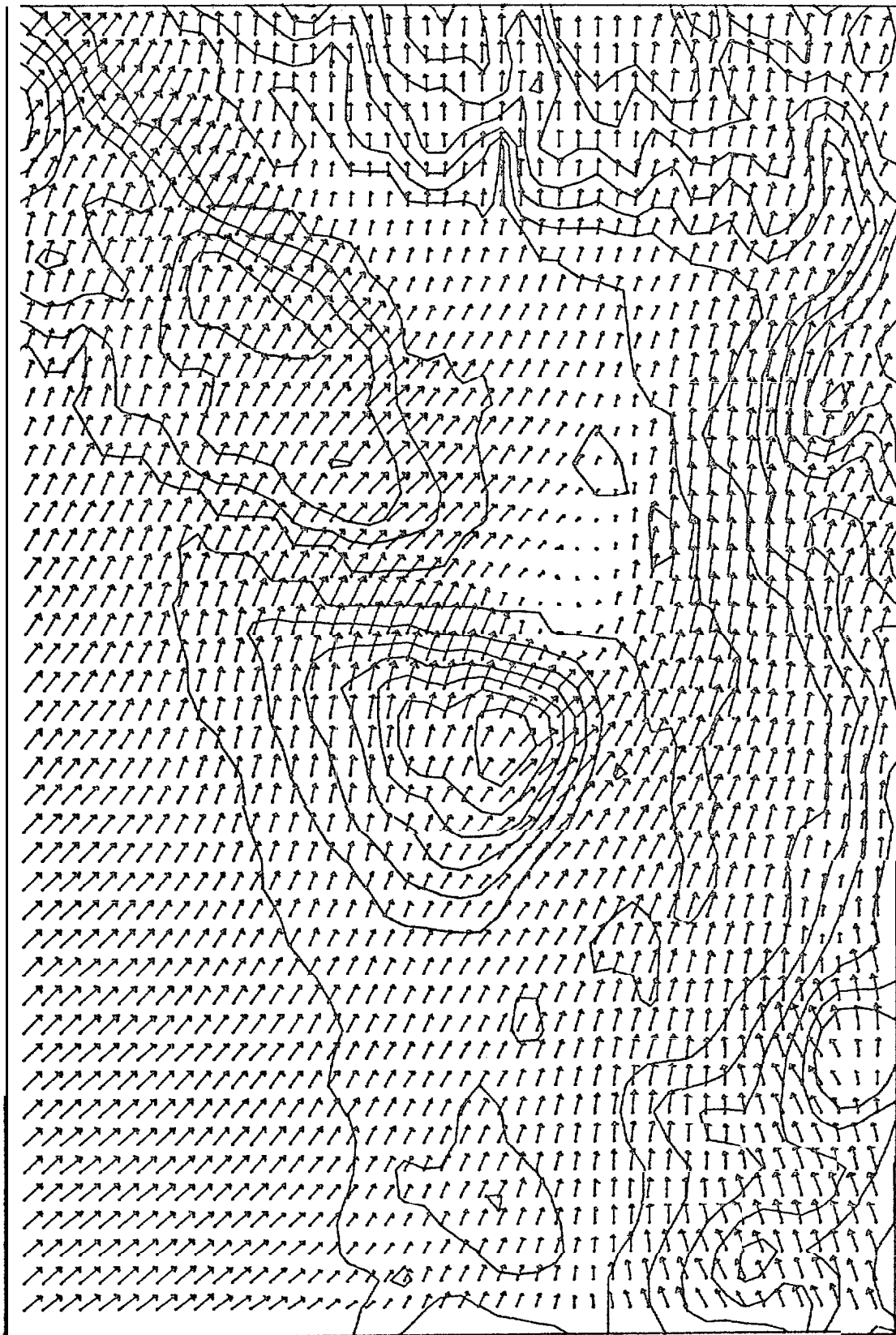
$$V_g = 10 \text{ m/s at } 335^\circ \text{ for NW flow}$$

$$E = 0.$$

The background large scale pressure gradient F_i is calculated to balance the specified geostrophic wind, V_g . The PBL height is initialized by h_i and velocities are initialized at 70% of the geostrophic wind.

Figures 4a and 4b show the calculated wind field and deviation of boundary layer height from h_i for the southwest wind case. Elevation contours are approximately 250m intervals. The deviation heights are dashed lines with a 200m contour interval. From the wind vectors one

VELOCITY VECTOR PLOT



10 METERS PER SECOND

Figure 4a. Boundary layer winds for southwest geostrophic flow.

BOUNDARY LAYER HEIGHTS

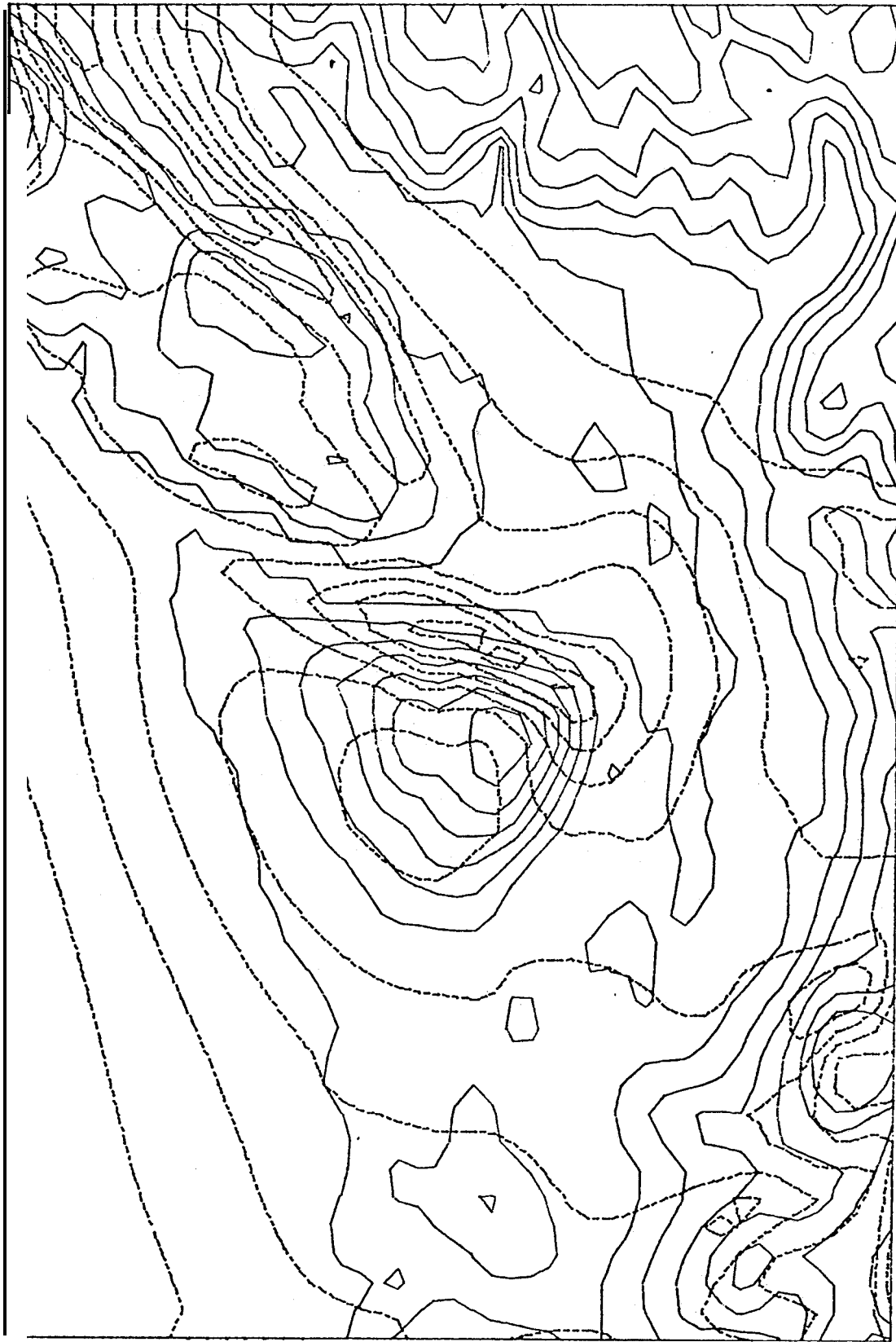


Figure 4b. Deviation of boundary layer height from the open ocean reference height as shown by dashed lines. Broad local maximums are on the windward side of Vancouver Island and the Olympic Mountains. Sharp minimums are to the N.E. of these same features.

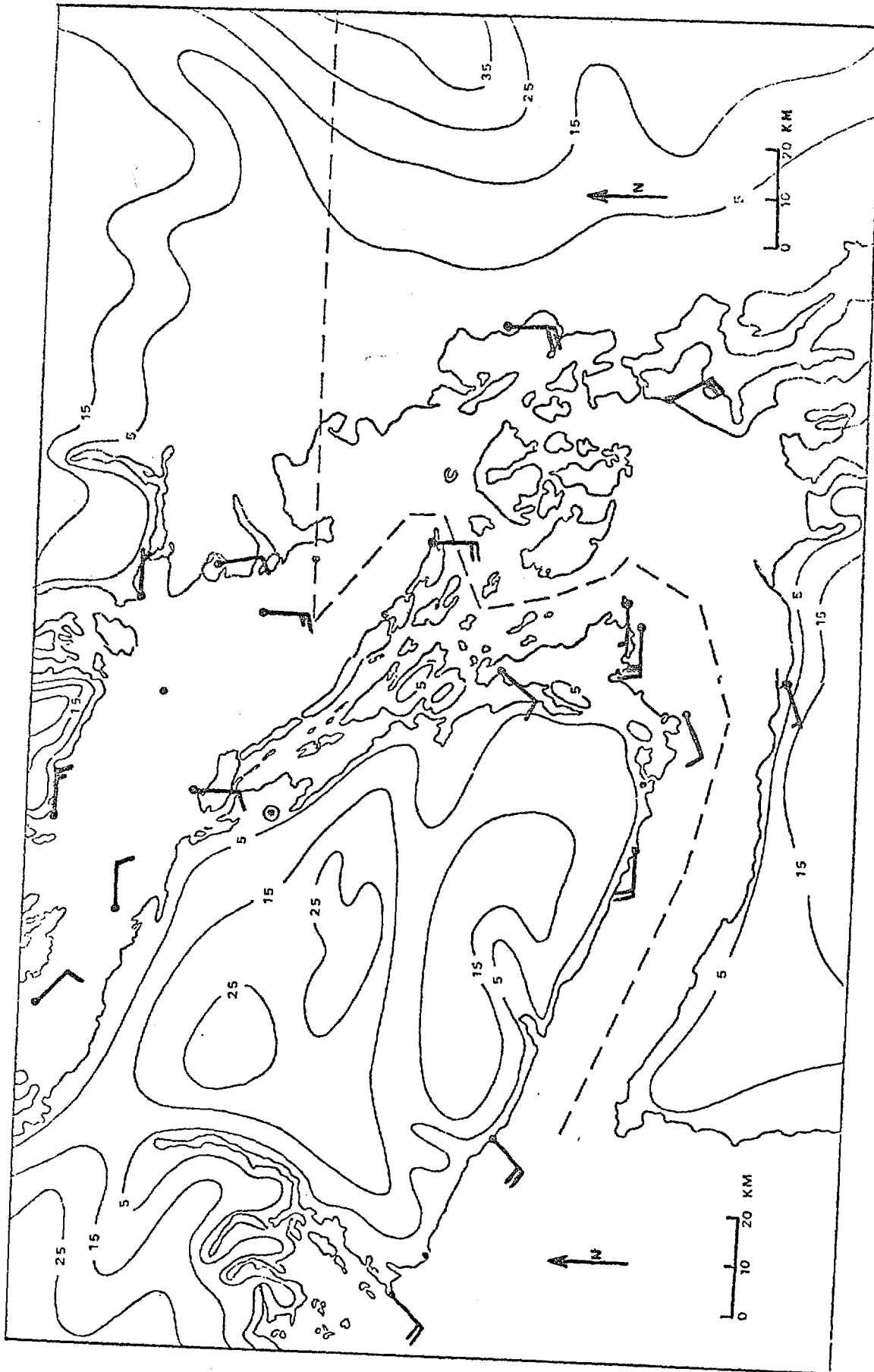
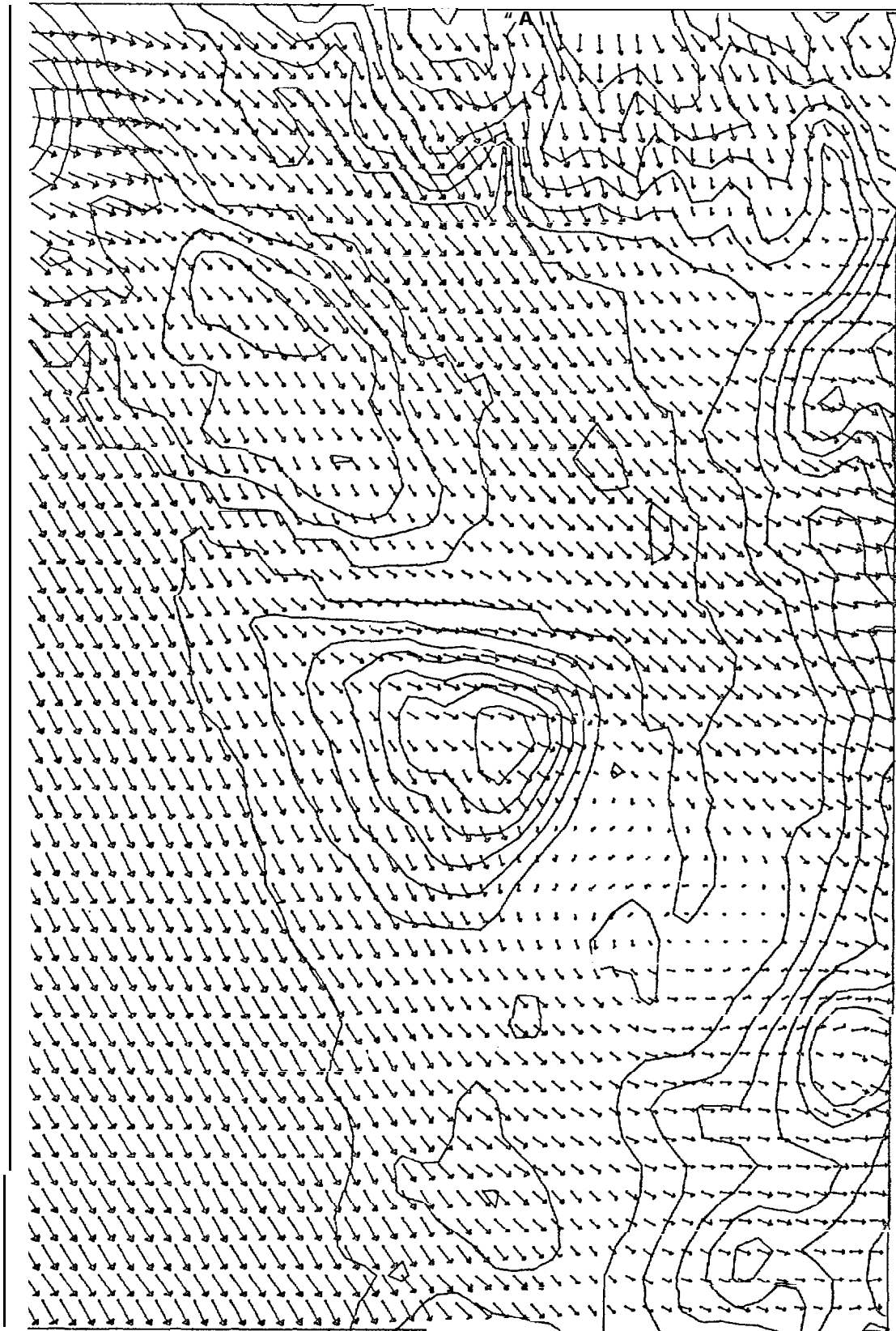


Figure 5. Reported winds for 0300-0400 GMT 25 October 1973. Sea level geostrophic wind is 13 m/s from 240°. Long wind barb is 10 kts and short barb is 5 kts (after Danard 1975.)

VELOCITY VECTOR PLOT



10 METERS PER SECOND

Figure 6a. Boundary layer winds for northwest flow.

BOUNDARY LAYER HEIGHTS

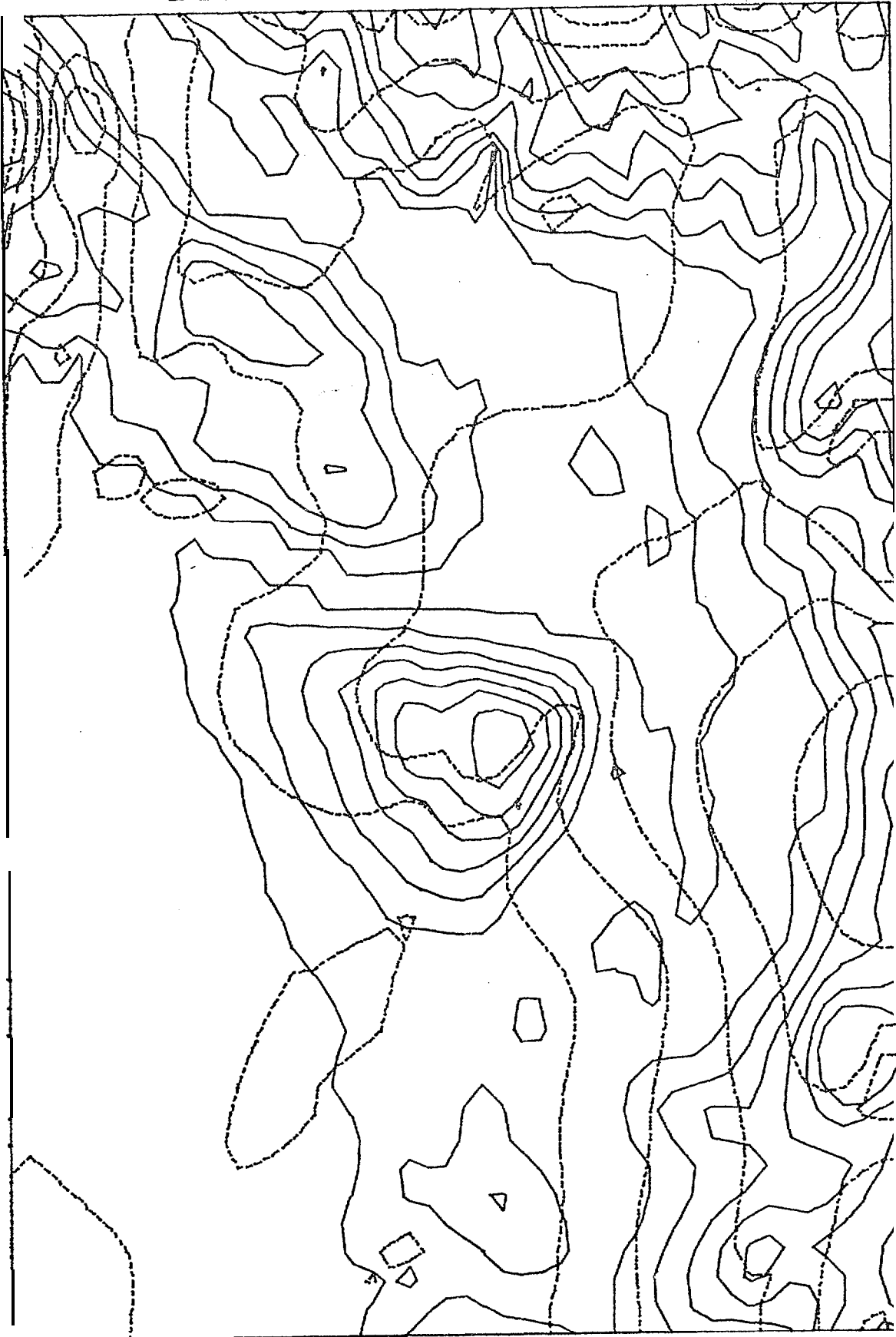


Figure 6b. Deviation of boundary layer height.

first notices that the flow is channeled by the Olympic Mountains. Winds over Puget Sound stronger and more southerly than off shore. Nearshore winds along the south coast of Vancouver Island and near the entrance to the Strait of Juan de Fuca are more southerly than farther off shore. The Strait of Georgia shows a large variation of local wind between the northern and southern end. Increased winds flow through the low point in the mountains of Vancouver Island and spill out over the inland waters. An eddy has formed at the east end of the Strait of Juan de Fuca near Port Angeles. The PBL deviations show a gentle rise over the windward side of the mountains with a pronounced lee wave trough on the downwind side of the Olympics and Vancouver Island.

For comparison, Fig. 5 gives observed anemometer winds at selected coastal stations which closely correspond to the synoptic situation depicted in Fig. 4a. As with the model, observed winter SW flow has strong winds along the east side of Puget Sound, with reduced flow in the region southeast of Vancouver Island. Winds at Victoria are less intense and more westerly than the model suggests. It may be that the position of the eddy and the magnitude of the pressure gradient that develops along the axis of the Strait of Juan de Fuca is very sensitive to the volume of air channeled through Puget Sound, which depends in turn on the orientation of the offshore flow.

Fig. 6a and 6b show velocity and height deviation for northwest winds. Channeling is indicated in the Strait of Juan de Fuca and especially by the Strait of Georgia. Height deviations are less intense than for the southwest wind case although the velocity field

indicates that the lee wave eddy is still a major feature.

In contrasting the wind and height fields for the two cases, northwest winds flow fairly closely to the orientation of the ridge line. Southwest winds funnel flow into Puget Sound but farther north inertia carries the major volume flux, velocity multiplied by PBL depth, cross contour through the low points in the ridge crest which induces a major local response in the height field.

The preliminary experiments indicate several persistent meso-scale features in the Puget Sound region. We can anticipate several important aspects. For offshore winds in the south to southwest quadrant one expects coastal winds and winds in Puget Sound to have a rather high coherency. Winds in the Strait of Juan de Fuca are very sensitive to adjacent terrain features. Direct over water measurements from the Straits will be very basic in understanding the induced flow patterns.

a

IV-3. Simulation of the Yukutat Region of Alaska

A location map for the Yukutat region, along the southeastern Alaska is shown in Fig. 7. Coastal modification along this coast is generally extensive enough to seriously affect estimates of surface winds for the region.

Little definitive exploration of the local meteorology of this region was accomplished before the study completed by Reynolds and Walter (1976). The data and cases shown in this section are based upon their recommendations.

The topographic grid is rectangular with a spacing of 5 km (Fig. 8). Other parameters are taken as:

$$f = 1.20 \times 10^{-4} / \text{sec}$$

$$g = 981.0 \text{ cm/sec}^2$$

$$\theta_n = 3^\circ \text{K}$$

$$\theta_i = 274.^\circ \text{K}$$

$$\theta_s = 282^\circ \text{K (water)}$$

$$\theta_s = 274.^\circ \text{K (land)}$$

$$CD = 1.3 \times 10^{-3} \text{ (water)}$$

$$C_H = 5.0 \times 10^{-3} \text{ (land)}$$

$$h_i = 1.1 \text{ km}$$

$$V_g = 12 \text{ m/s at } 135^\circ \text{ and } 355^\circ$$

Note that a significant land water contrast in surface temperature is considered.

The results of the two cases of different prevailing winds are shown in Fig. 9 and 10. There are three major drainage regions easily

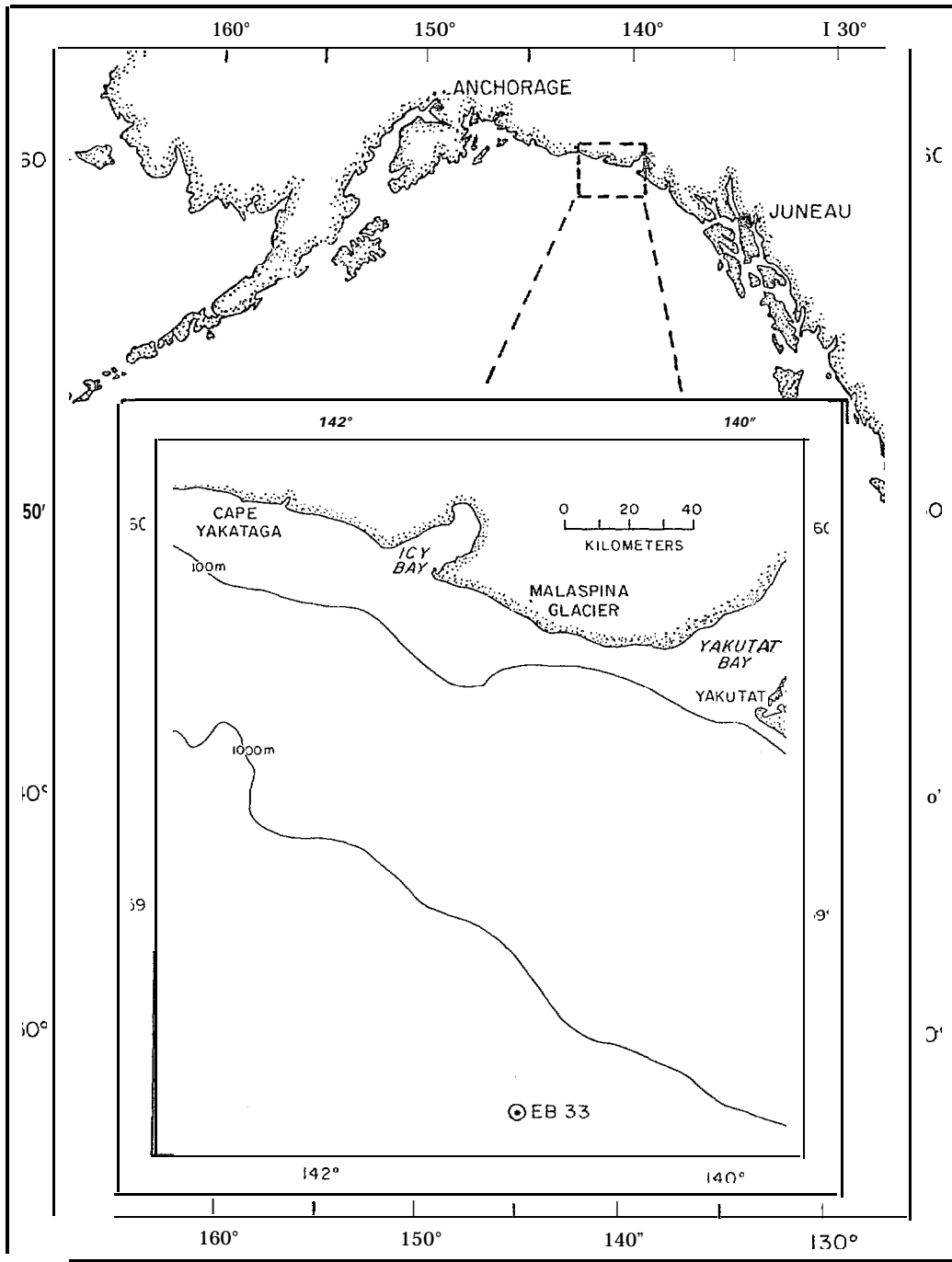


Figure 7. Location map for southeast Alaska.

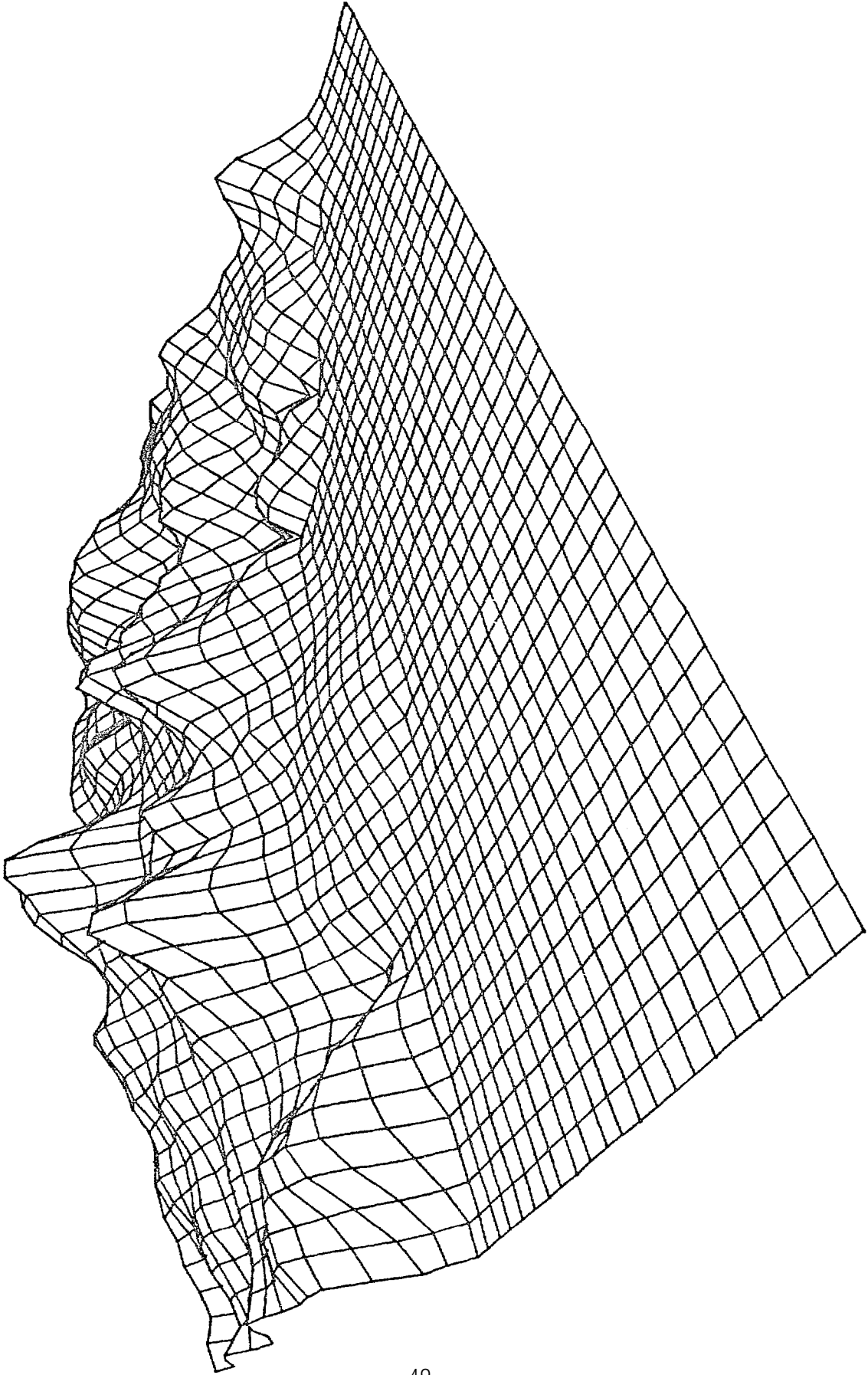
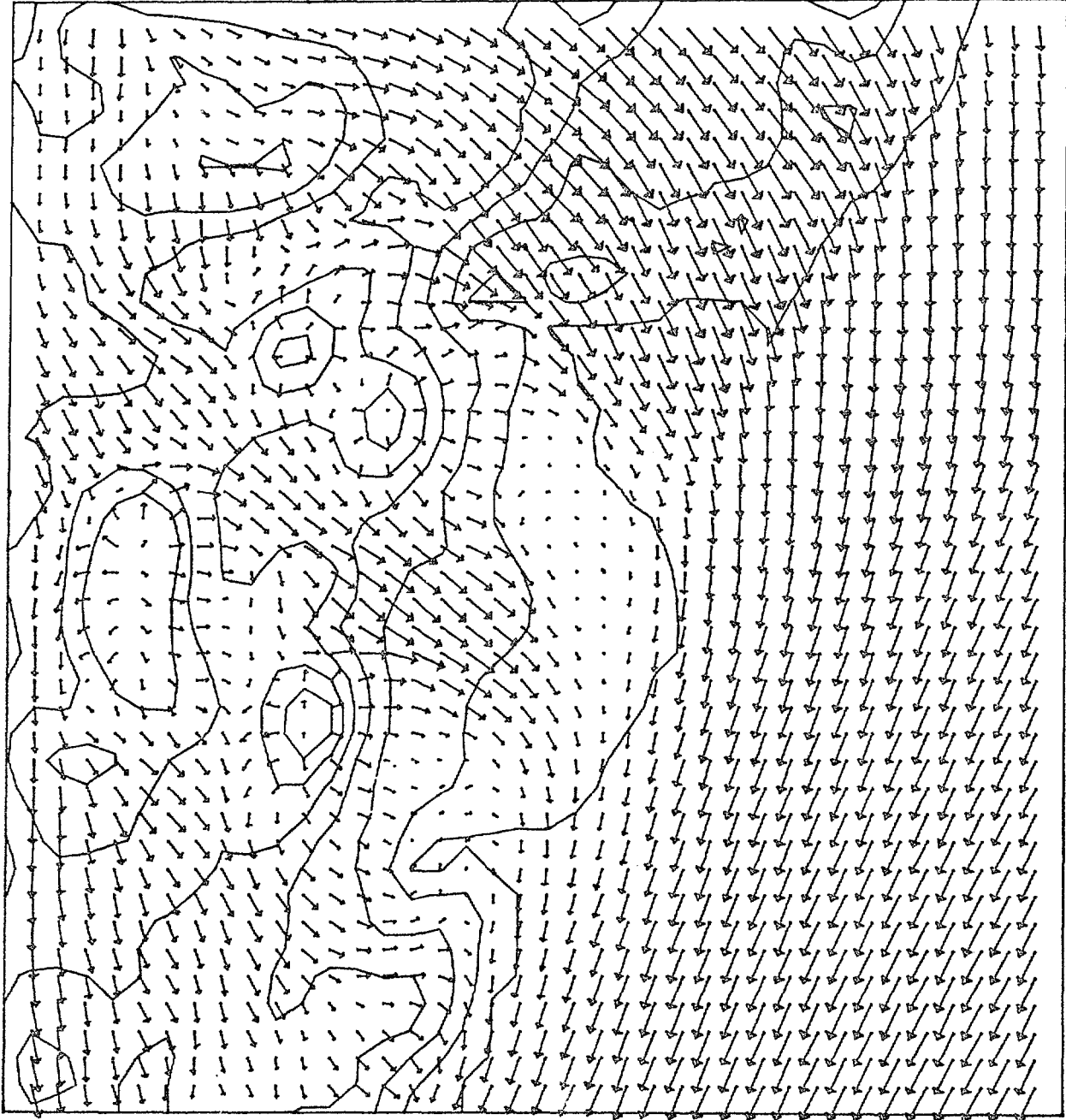


Figure 8. Topographic grid for Yukutat region as viewed from the west

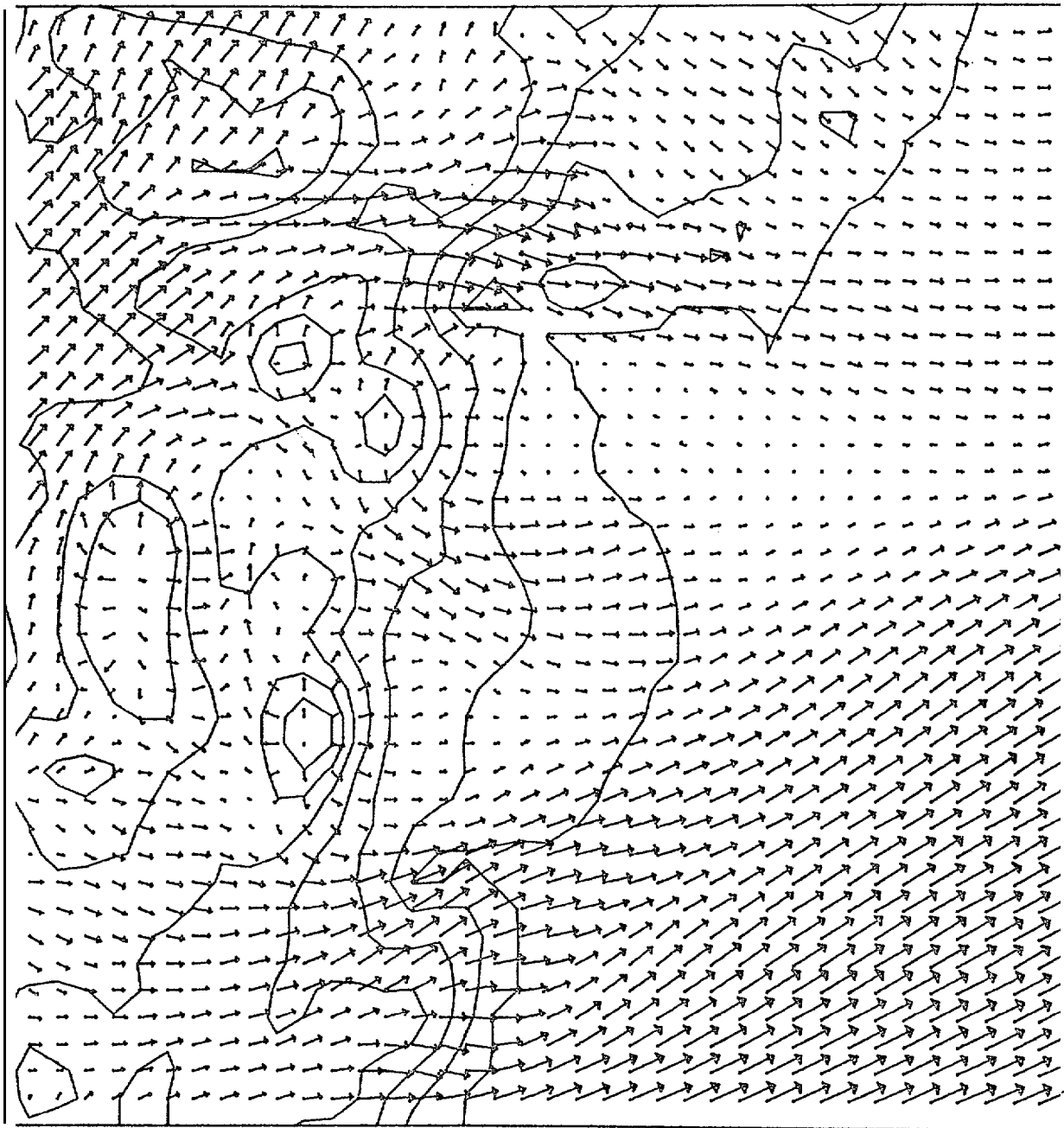
V L L U U I I V L L U U I I L U I



10 METERS PER SECOND

Figure 9. Geostrophic wind at 135° relative to top of figure at 13 m/s.

VELOCITY VECTOR PLOT



0 METERS PER SECOND

Figure 10. Geostrophic wind at 155° relative to top of figure at 13 m/s.

visualized in Fig. 8, separated by the major mountain peaks. In Fig. 9 for example, there are strong offland flow near Yukutat and across the Malaspina Glacier oriented nearly 90 to the unobstructed flow shown in the southwest corner. For northwest winds (Fig. 10) there are channeled winds in the Icy Bay area and suggestions of an eddy in the vicinity of Yukutat. Both cases show extensive channeling and horizontal wind shear south of Yukutat, one of the main regions of anomalous winds indicated by the Coast Guard in Fig. 1.

By way of comparison, we reproduce Fig. 11 from Reynolds and Walter (1976) showing a sequence of offshore wind measurements made in November 1975. This data is roughly consistent with the 135 case shown in Fig. 9. Fig. 11 does not show the extent of over water influence near the Glacier as indicated by the measurements.

It is now apparent that one must take a closer evaluation of the contrast between the land and ice as well as land and water.

IV-4. Conclusions

It is obvious from the lack of direct verification and smoothness of some of the fields that further analysis is needed in each region for model results to be directly applied. However, the model has fulfilled its original goal of dynamic exploration and suggesting important regional patterns. The model is at the stage where it can be used as an aid to field observations in making an assessment of regional flow patterns near Icy Bay.

Its easy adaptability to any area makes the model an important

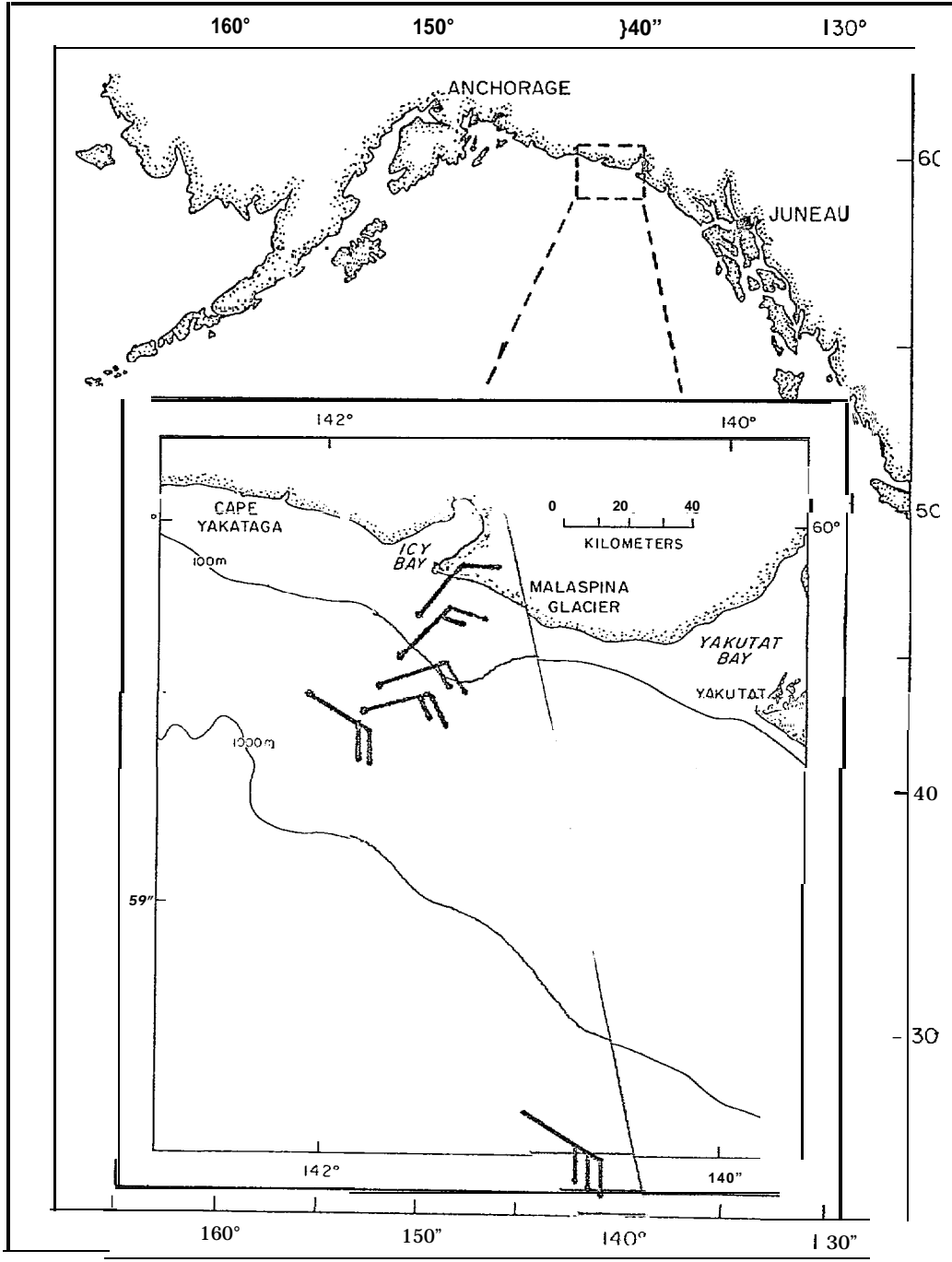


Figure 11. Icy Bay wind stations for geostrophic flow approximately 150° at 13 m/s (after Reynolds and Walter, 1976).

tool in recommending key locations for direct observations at other locations along the Alaskan coast.

SECTION V. BERING SEA MODEL

v-1. Introduction

The circulation of the Bering Sea is of particular interest because the region has great potential for the natural resources related industries such as fisheries, offshore mining industries, etc., and a thorough understanding of the current system in the sea is essential for the environmental assessment studies of the area.

Extensive studies of hydrographic data and a limited number of direct measurements indicate that the major currents in the sea are mainly driven by wind forcing, thermohaline forcing, interactions with the Pacific Ocean through numerous open passes along the Aleutian chain, and, to a limited extent, interactions with the Arctic Ocean through the Bering Strait. In addition, the bathymetry of the sea has been recognized as an important dynamical constraint. Our main effort has been to investigate the full, three dimensional structure of the currents **using a numerical general circulation model which** is sophisticated enough to include the above features. At the same time, we have constructed a simple diagnostic model to explore a certain aspect of the current system in the Bering Sea. We have made some preliminary calculations with this simple model. A brief review of the model and results is the subject of this report. A brief discussion of the mathematical model is presented in Section 2, together with the boundary conditions. Some preliminary results and their implications are discussed in Section 3.

V-2. The Mathematical Model and Boundary Conditions

a. Model

The equations of motion for horizontal non-accelerated flow with a constant vertical eddy coefficient are:

$$-fv\rho_0 = -\frac{1}{a \cos\phi} \frac{\partial p}{\partial \lambda} + \kappa \frac{\partial^2 u}{\partial z^2} \quad (1)$$

$$fu\rho_0 = -\frac{1}{a} \frac{\partial p}{\partial \phi} + \kappa \frac{\partial^2 v}{\partial z^2} \quad (2)$$

The hydrostatic equation and the mass continuity equation are:

$$\frac{\partial p}{\partial z} = -g\rho_0 \quad (3)$$

$$\frac{1}{a \cos\phi} \frac{\partial u}{\partial \lambda} + \frac{1}{a \cos\phi} \frac{\partial}{\partial \phi} (v \cos\phi) + \frac{\partial w}{\partial z} = 0 \quad (4)$$

In these equations spherical coordinates are used, with λ , ϕ , and z representing longitude, latitude, and height. The fluid is contained between the surface $z = \eta$ and the bottom $z = -H(\lambda, \phi)$. The model specifies two horizontal velocities and the pressure. The model assumes the fluid is homogeneous, thus the density ρ_0 is a constant ($\rho_0 = 1$.)

The boundary conditions are:

$$\kappa \rho_0 \frac{\partial u}{\partial z} = \tau_{\lambda}^{\phi}, \quad \kappa \rho_0 \frac{\partial v}{\partial z} = \tau_{\phi}^{\lambda} \quad \text{and} \quad W = \left(\frac{u}{a \cos\phi} \frac{\partial \eta}{\partial \lambda} + \frac{v}{a} \frac{\partial \eta}{\partial \phi} \right) \quad \text{at } z = \eta \quad (5)$$

$$\kappa \rho_0 \frac{\partial u}{\partial z} = \tau_b^{\lambda}, \quad \kappa \rho_0 \frac{\partial v}{\partial z} = \tau_b^{\phi} \quad \text{and} \quad W = -\left(\frac{u}{a \cos\phi} \frac{\partial H}{\partial \lambda} + \frac{v}{a} \frac{\partial H}{\partial \phi} \right) \quad \text{at } z = -H(\lambda, \phi) \quad (6)$$

In (5) and (6) η is the free surface elevation; H is the depth of the ocean; and τ_b^{λ} and τ_b^{ϕ} are the bottom stress components. Assuming that $\eta/H \ll 1$, we impose the boundary condition (5) at $z = 0$. Then the momentum equation (1) and (2) are vertically averaged to yield:

$$-f\bar{v} = -\frac{g}{a \cos\phi} \frac{\partial n}{\partial \lambda} + \frac{1}{H} (\tau_o^\lambda - R\bar{u}), \quad (7)$$

$$f\bar{u} = -\frac{g}{a} \frac{\partial n}{\partial \phi} + \frac{1}{H} (\tau_o^\lambda - R\bar{v}) \quad (8)$$

where

$$u = \frac{1}{H} \int_{-H}^0 \rho_o u dz \quad (9)$$

$$v = \frac{1}{H} \int_{-H}^0 \rho_o v dz \quad (10)$$

In (7) and (8) the component bottom stresses are taken as $R\bar{u}$ and $R\bar{v}$ where R is the coefficient of friction.

Integration of the continuity equation (4) with boundary conditions (5) and (6) yields:

$$\frac{1}{a \cos\phi} \frac{\partial}{\partial \lambda} \left(\int_{-H}^0 u dz \right) + \frac{1}{a \cos\phi} \frac{\partial}{\partial \phi} \left(\cos\phi \int_{-H}^0 v dz \right) = 0 \quad (11)$$

Equation (11) simply states that the vertically integrated flow is horizontally nondivergent, which guarantees the existence of a stream function ψ such that

$$\bar{u} = \frac{1}{H} \int_{-H}^0 u dz = -\frac{1}{a} \frac{1}{H} \frac{\partial \psi}{\partial \phi} \quad (12)$$

$$\bar{v} = \frac{1}{H} \int_{-H}^0 v dz = \frac{1}{H} \frac{1}{a \cos\phi} \frac{\partial \psi}{\partial \lambda} \quad (13)$$

Substituting (12) and (13) into (7) and (8), and applying the cur_z operator, defined by

$$\text{cur}_z (q_1, q_2) = \frac{1}{a \cos\phi} \frac{\partial q_2}{\partial \lambda} - \frac{\partial q_1}{\partial \phi} \quad (q_1 \cos\phi) \quad (14)$$

and simplifying by eliminating a factor of $1/(a^2 \cos\phi)$, we get:

$$\begin{aligned}
R \frac{\partial}{\partial \lambda} \left(\frac{1}{H^2 \cos \phi} \frac{\partial \psi}{\partial \lambda} \right) + \frac{\partial}{\partial \phi} \left(\frac{\cos \phi}{H^2} \frac{\partial \psi}{\partial \phi} \right) + \frac{\partial}{\partial \phi} \left(\frac{f}{H} \right) \frac{\partial \psi}{\partial \lambda} - \frac{\partial}{\partial \lambda} \left(\frac{f}{H} \right) \frac{\partial \psi}{\partial \phi} \\
= \frac{\partial}{\partial \lambda} \left(\frac{\tau_o^\phi}{H} \right) - \frac{\partial}{\partial \phi} \left(\frac{a \cos \phi}{H} \tau_o^\eta \right) \quad (15)
\end{aligned}$$

Eq. (15) is an inhomogeneous, linear, elliptic, second-order partial differential equation for the stream function ψ . For a given bathymetry $H(\lambda, \phi)$ and a prescribed surface stress distribution $\tau_o^\lambda(\lambda, \phi)$, $\tau_o^\phi(\lambda, \phi)$ it can be solved **numerically by the relaxation method**. It should be noted, however, that the highest order terms involve a small friction parameter R , and thus special care must be taken to maintain stability of the numerical method. This will be discussed in (c).

b. Surface Wind Stress and Open Boundary Conditions

Wind stress can be estimated by conventional drag law methods if the surface wind is known. Unfortunately, wind measurements over the Bering Sea are very sparse in space and time, since they generally come from a handful of ship stations. For the numerical model, therefore, wind stress is computed from surface pressure data. First, monthly mean pressure data provided by the National Climate Center, was interpolated quadratically from $5^\circ \times 5^\circ$ grid mesh into the model grid mesh 2° (long.) \times 1° (lat.). The interpolated pressure data was then used to estimate geostrophic wind velocity, and the wind velocity at anemometer height was obtained by multiplying the geostrophic wind speed by a factor γ and changing the geostrophic wind direction by an angle α . The constant γ here is 0.7 while α is 19° .

variable part of the pressure could increase the wind stress estimate through the non-linearity of the drag law. In fact, the study by Aagaard (1970) strongly suggests that the stress computed from the monthly mean pressure could be easily underestimated by a factor of 2 or 3. On the basis of this study, we multiplied the monthly mean stress by 3.0 for the model calculation.

The annual mean wind stress was computed by averaging 12 months of wind stress data. This is shown in Figure (1). The computed monthly mean wind stress patterns for January and August are shown in Figures (2) and (3). The January map shows a typical winter pattern which is characterized by the northeasterly stress associated with a strong high pressure center over Siberia and a low pressure center over the North Pacific Ocean. On the other hand, the stress pattern in August (Figure (3)) shows a very weak stress over most of the sea, and somewhat stronger southwesterly stress over the southeast part of the basin. In general, the wind forcing in summer is weaker in order of magnitude than in winter.

At the open boundaries of the grid, estimates of vertically integrated transports are required. The model has four open boundaries along the Aleutian - Commander Island Arc: Kamtchatka Strait, Commander - Near Strait, Central Aleutian pass and Western Aleutian Pass. Also the Bering Strait is modelled as an open boundary. The widths and depths of the open boundaries are adjusted to match the observed bathymetry within the limits imposed by grid resolutions.

WINDSTRESS VECTOR PLOT

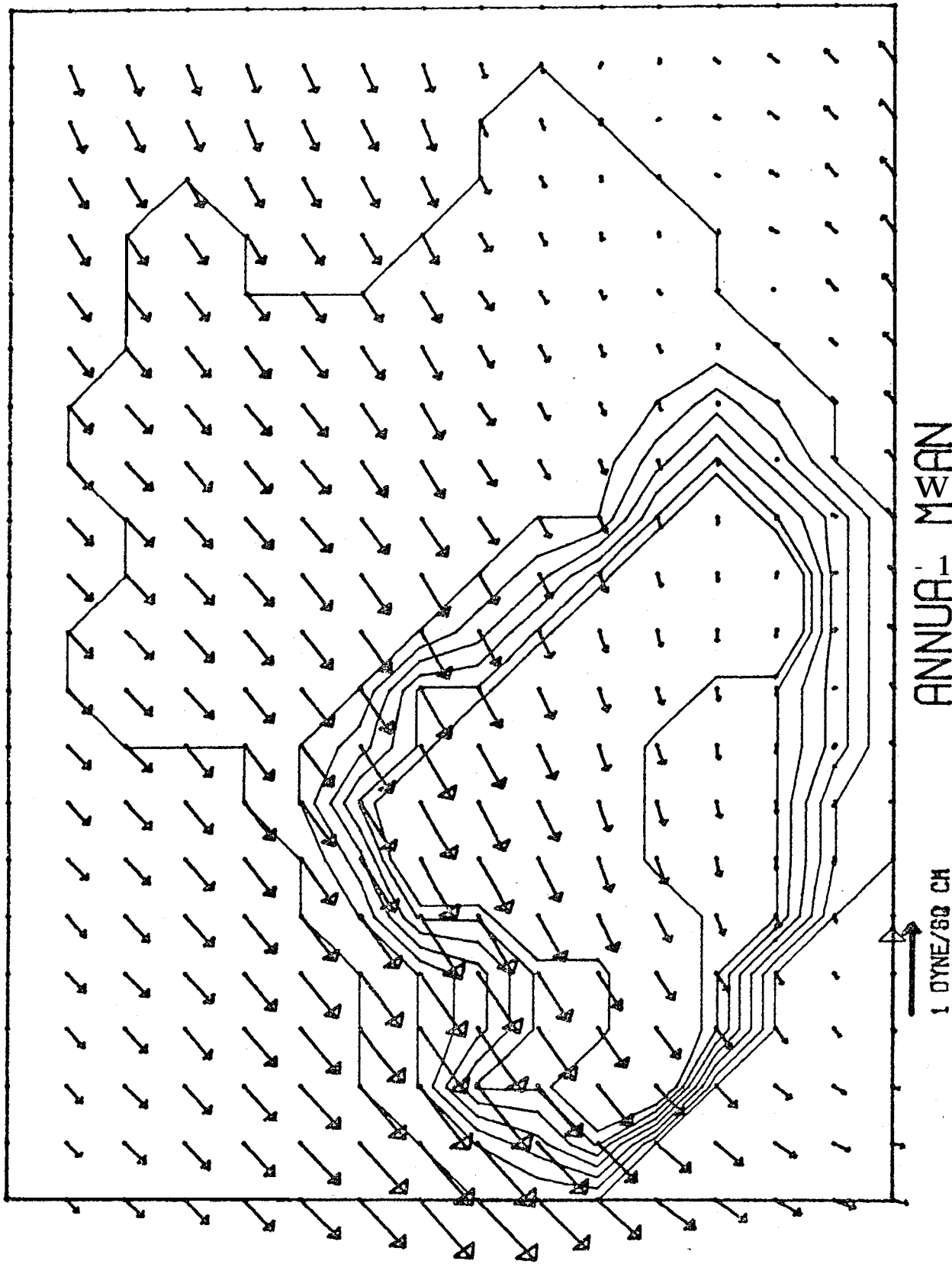
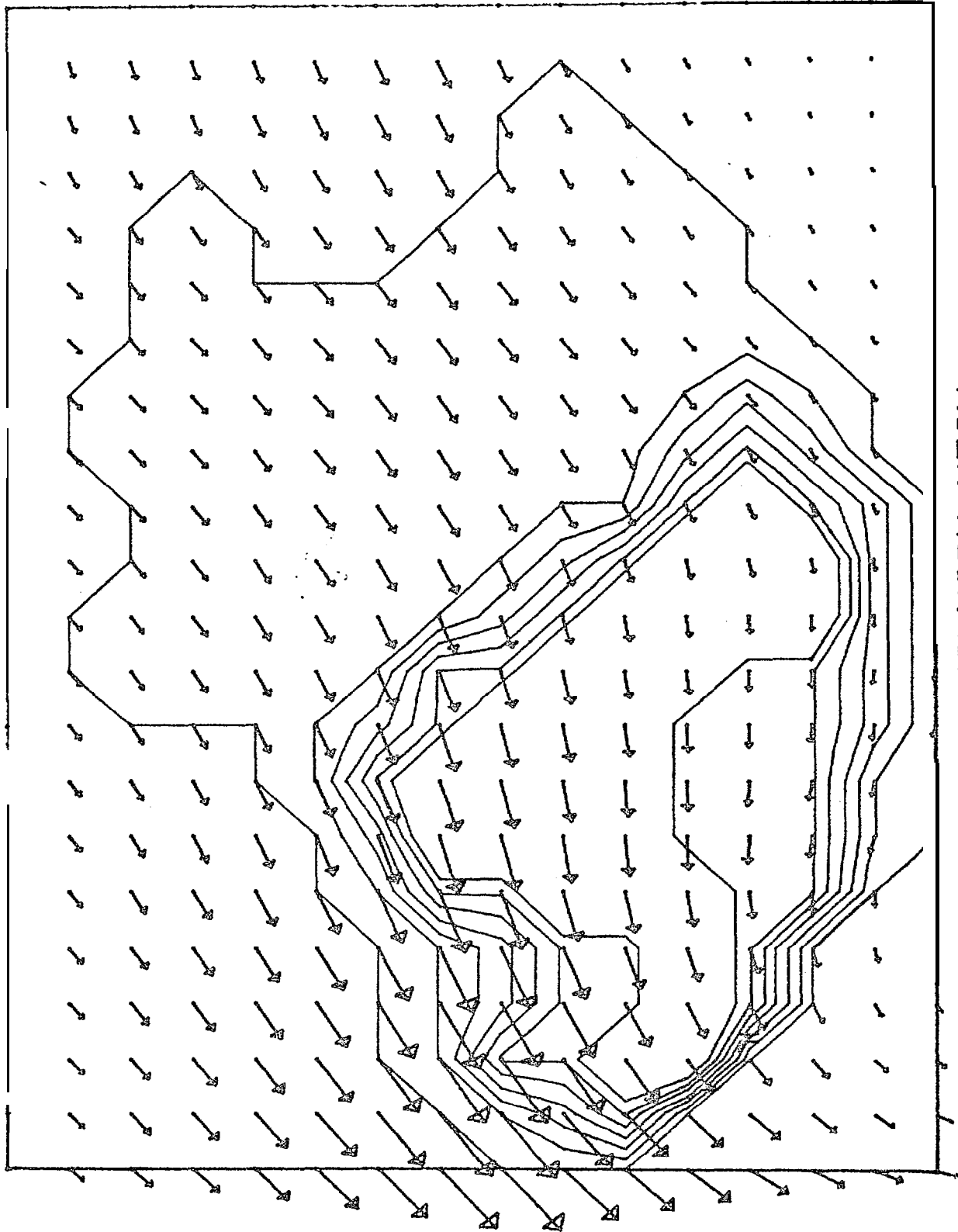


Figure 1. Annual mean wind stress vector plot for the Bering Sea.

WINDSTRESS VECTOR 12-0T



JANUARY MEAN

→ 1 DYNE/CM²

Figure 2. January mean wind stress vectors for the Bering Sea.

WIND STRESS VECTOR PLOT

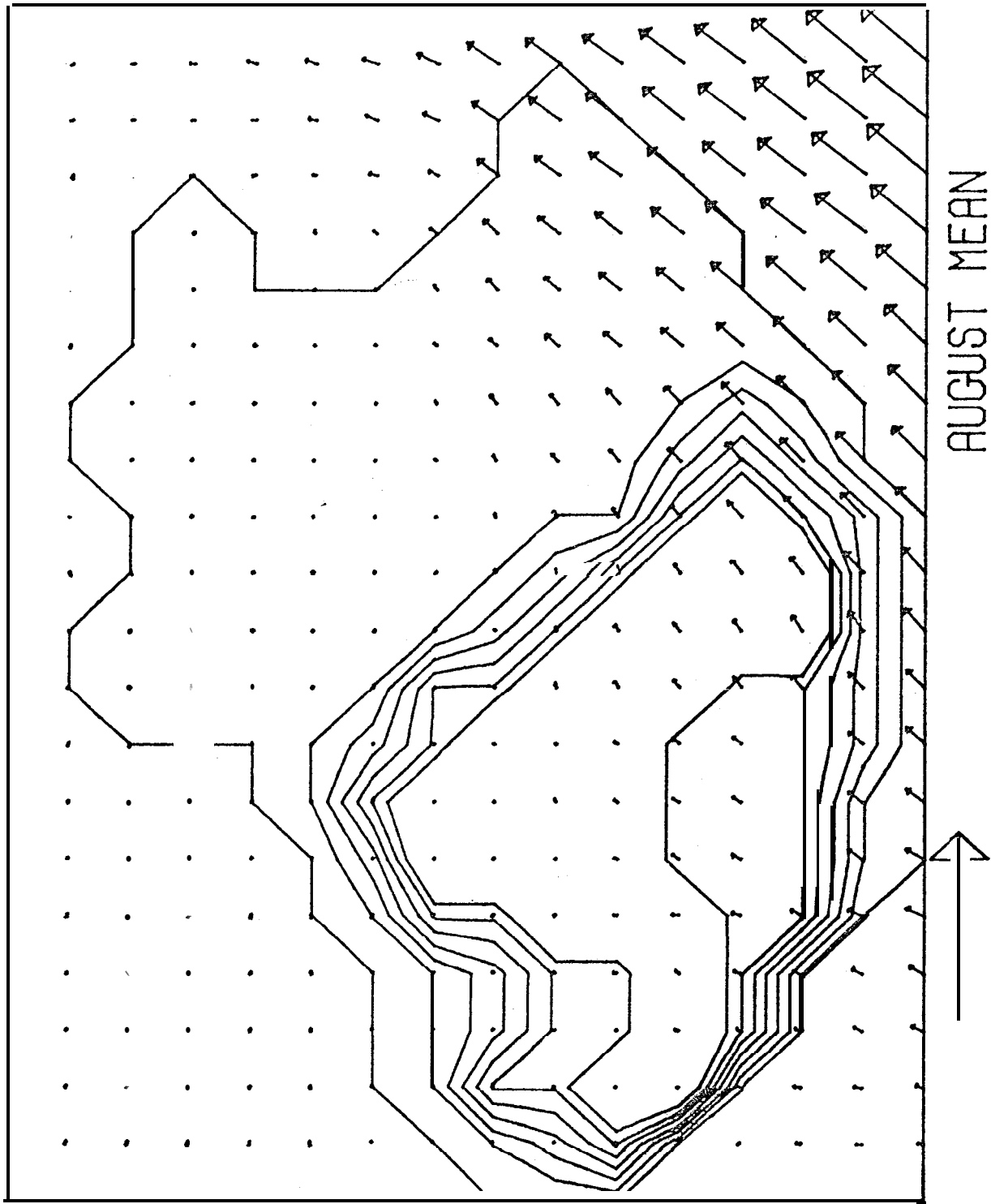


Figure 3. August mean wind stress vectors for the Bering Sea.

Integrated volume transport values on the open sections are chosen from various estimates presently available. It should be mentioned however, that at the present stage, there are many uncertainties in transport estimates at the various passes.

The chosen values of **(annual mean) transports** are given in Table (I). A net transport of 18sv outward through the Kamtchatka Strait is in close agreement with an estimate of 18.4sv by Arsenev (1967) and summer values (20sv) by Hughes et al , (1974). A net transport of 14sv inward across the commander - near Strait was taken from Arsenev (1967) which is greater than an estimate (10SV) by Favorite (1974) but less than Hughes et al (25sv). The total inflows through the Western and Central Aleutian are based on the estimates made by Arsenev (1967). For the Bering Strait, the total transport (1sv) outward was chosen from the estimate (1.1sv) by Arsenev (1967).

c. Numerical Procedures

We write the basic equation (15) in a compact form using Cartesian coordinate:

$$R\Delta^2 \psi + A \frac{\partial \psi}{\partial x} + B \frac{\partial \psi}{\partial y} = \phi \quad (16)$$

where we denoted the right side of equation (15) ϕ . In (a) we have mentioned that Eq. (15) is the equation with small parameters at highest order terms. The shortcomings of the ordinary relaxation method for such an equation has been discussed by Sarkisian (1972) and Ilin (1969). For the present calculation, we adopted the method by

Table 1.

Mass transports at open boundaries

Kamchatka Strait	- 18sv.*
Commander - Near Strait	+ 14sv.*
Western Aleutian Pass	+ 4sv.
Central Aleutian Pass	+ 1sv.
Bering Strait	- 1sv.

* Outward

+ Inward

Sarkisian (1972) "method of directional differences". The essence of the method is quite simple: derivatives of the first order terms are substituted for the difference forward and backward, depending on the sign of coefficients, in such a way that diagonal terms possess maximum weights. The diagonal dominance of the matrix then guarantees convergence of the iteration method.

The only drawback of the method of directional difference is a computational viscosity. According to Sarkisian, however, the accuracy of the solution for a particular example is within 10% when it is compared with the solution obtained by a more accurate method by Marchuk (1973).

V-3. Results and Suggestions

Solutions were obtained first for the case of annual mean wind stress together with specified mass inflow - outflow along the boundary. Solution for each twelve month period were also obtained, but since the results are still in the process of verification, we will very briefly discuss a few sample calculations and defer detailed analysis for another report,

With an annual mean wind stress from the general direction of northeast, contours of the streamfunction for the whole Bering Sea Fig. (4) show a strong eye" onic gyre in the western half of the deep basin. Transport in the eastern shelf region is less than 2sv. (2×10^{10} m³/see). It is noted that the stream lines follow the bathy-

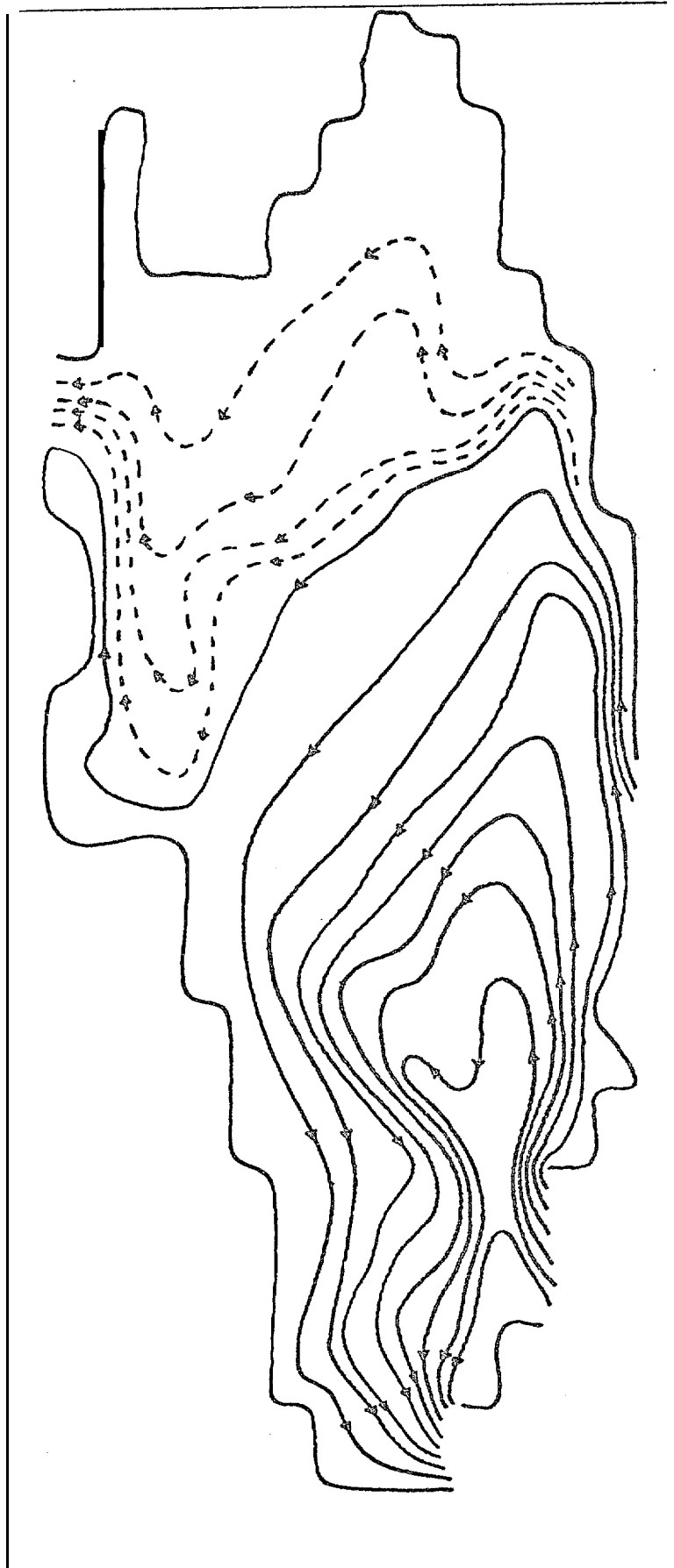


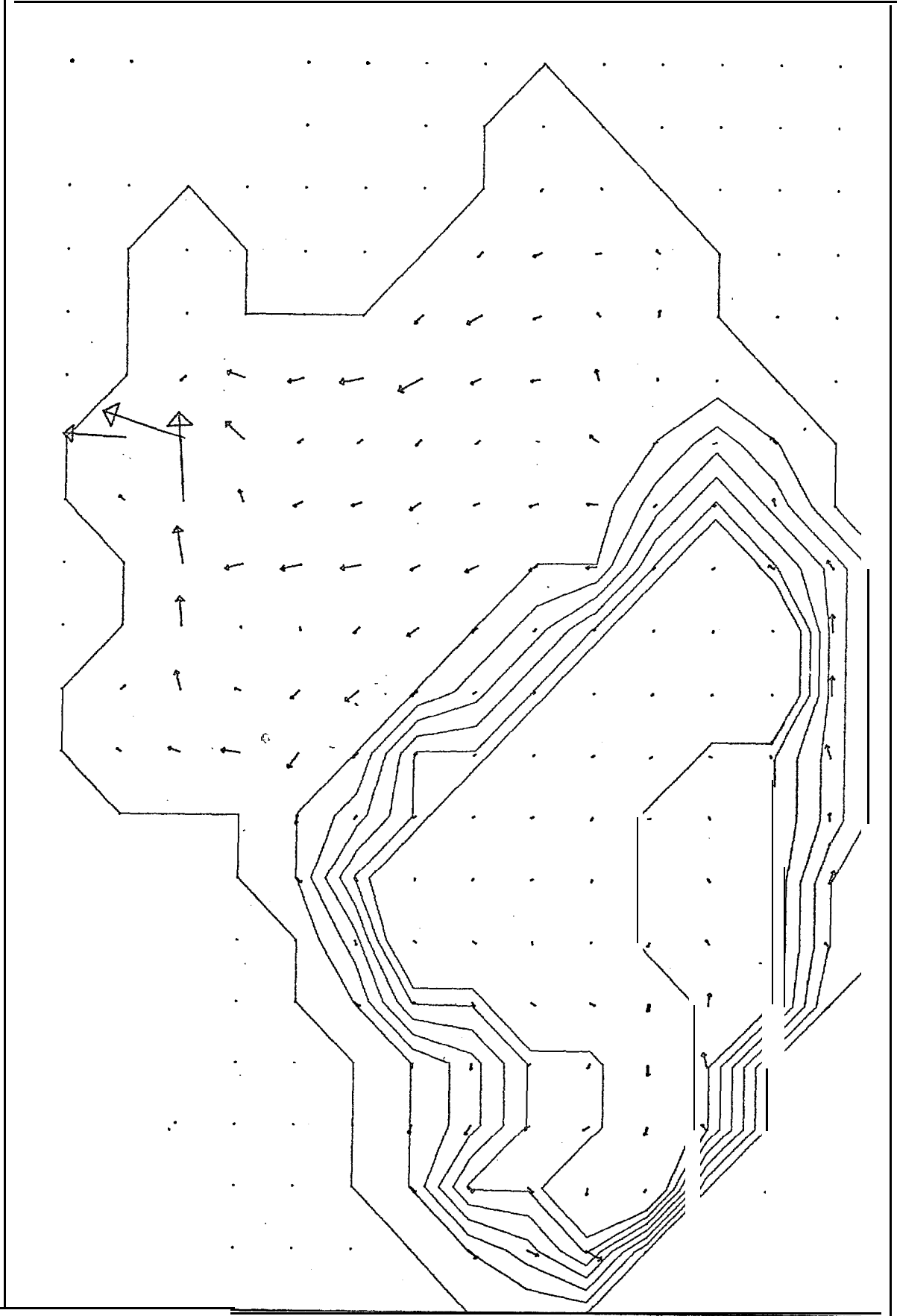
Figure 4. Circulation in the Bering Sea due to the annual mean wind with boundary source and sinks.

Transport Contours — 2.0 Sv ($10^8 \text{ m}^3/\text{sec}$)
 --- 0.2 Sv

metry closely, indicating a topographic control of the flow by the dynamic constraint of potential vorticity. Fig. (5) shows vertically averaged velocity vectors for the annual mean case. The flow speed over the shelf is significantly stronger than in the deep basin due to shallowness of the shelf. To show a clearer picture of the circulation pattern in the deep basin, that portion was magnified and is shown in Fig. (6). Again, the velocity vectors clearly show a tendency to follow the bathymetry. To illustrate the flow characteristics in two different seasons, sample calculations for January and August are shown in Fig. (7) and (8). Although the general cyclonic gyres in the deep basin are maintained in both seasons, the intensity of the cross basin transport along the shelf break is significantly different depending on the season. Furthermore, the deep basin circulation in January shows three closed gyres which are conspicuously absent in August.

To investigate the direct influences of wind forcing and sources and sinks separately, two controlled experiments were made; one with wind forcing (annual mean) only (Fig. 9), and the other one with a source-sink only (Fig. 10). It is interesting to note that the August circulation is very similar to the one with the source-sink only. This might indicate that the circulation in summer is primarily driven by the mass source-sink specified along the boundary. It is also noted that the closed gyres in the deep basin in January are direct consequences of wind forcing, which showed up clearly in the experiment with wind forcing only.

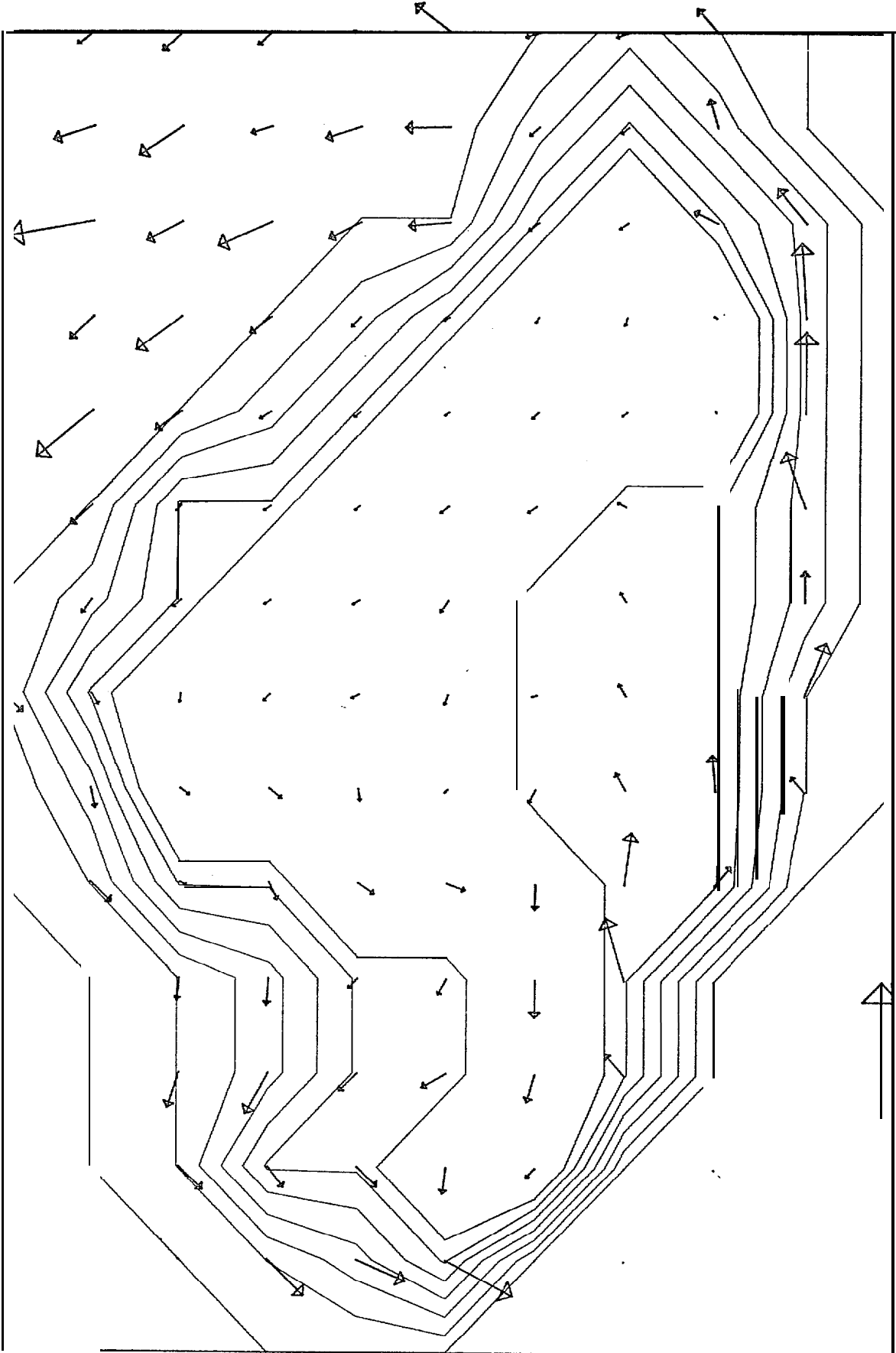
VELOCITY VECTOR PLI



100 METERS

Figure 5. Vertically averaged velocity vectors for the annual mean case in the Bermuda Sea.

VELOCITY VECTOR PLOT



10 CM PER

Figure 6. Circulation pattern for the deep basin in the Bering Sea for the annual mean case.

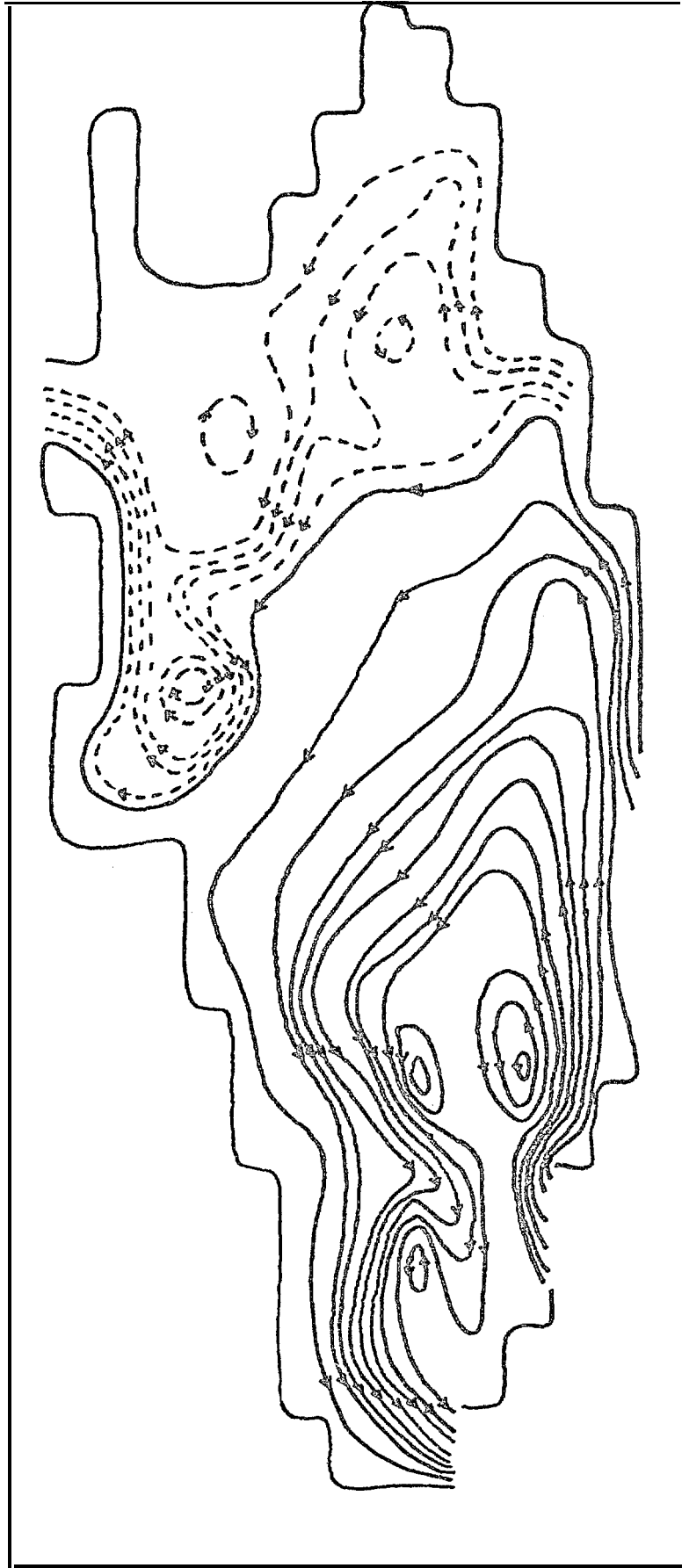


Figure 7. Circulation in the Bering Sea due to the January w' with boundary source and sinks.
 Transport Contours — 2.0 Sv ($10^6 \text{ m}^3/\text{sec.}$)
 --- 0.2 Sv

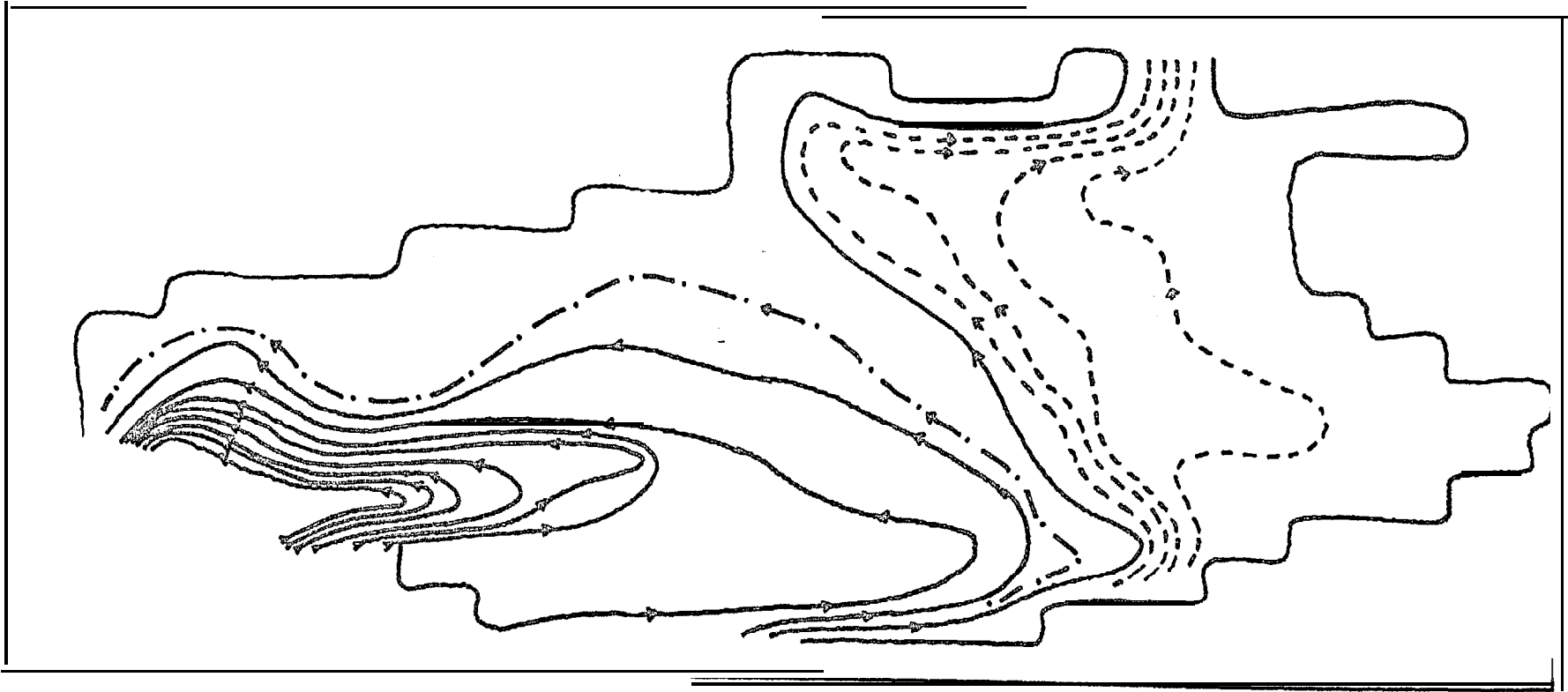


Figure 8. Circulation in the Bering Sea due to the August wind with boundary source and sinks.
Transport Contours -2.0 Sv ($10^6 \text{m}^3/\text{sec.}$)
--- 1.0 Sv
- · - 0.2 Sv

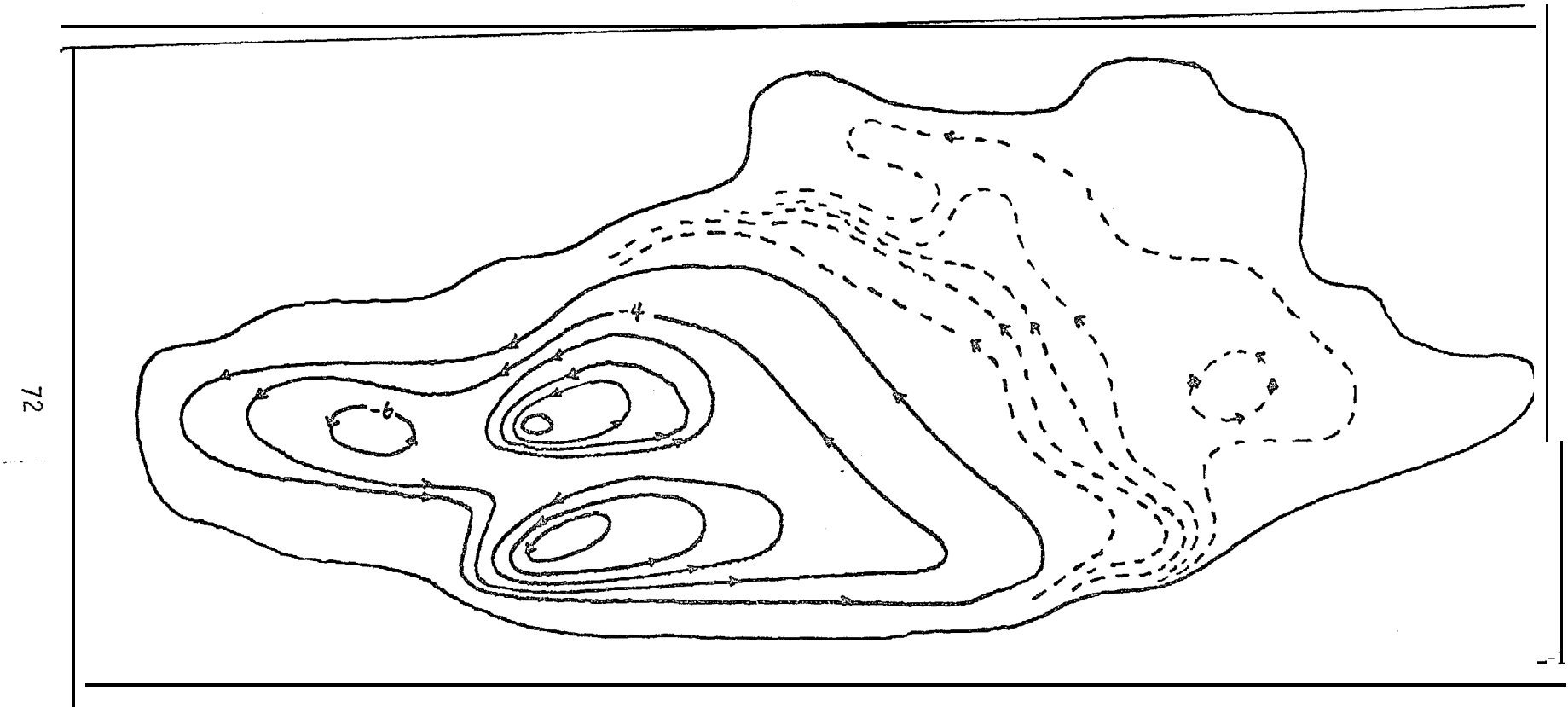


Figure 9. Circulation in the Bering Sea due to the annual mean wind only.

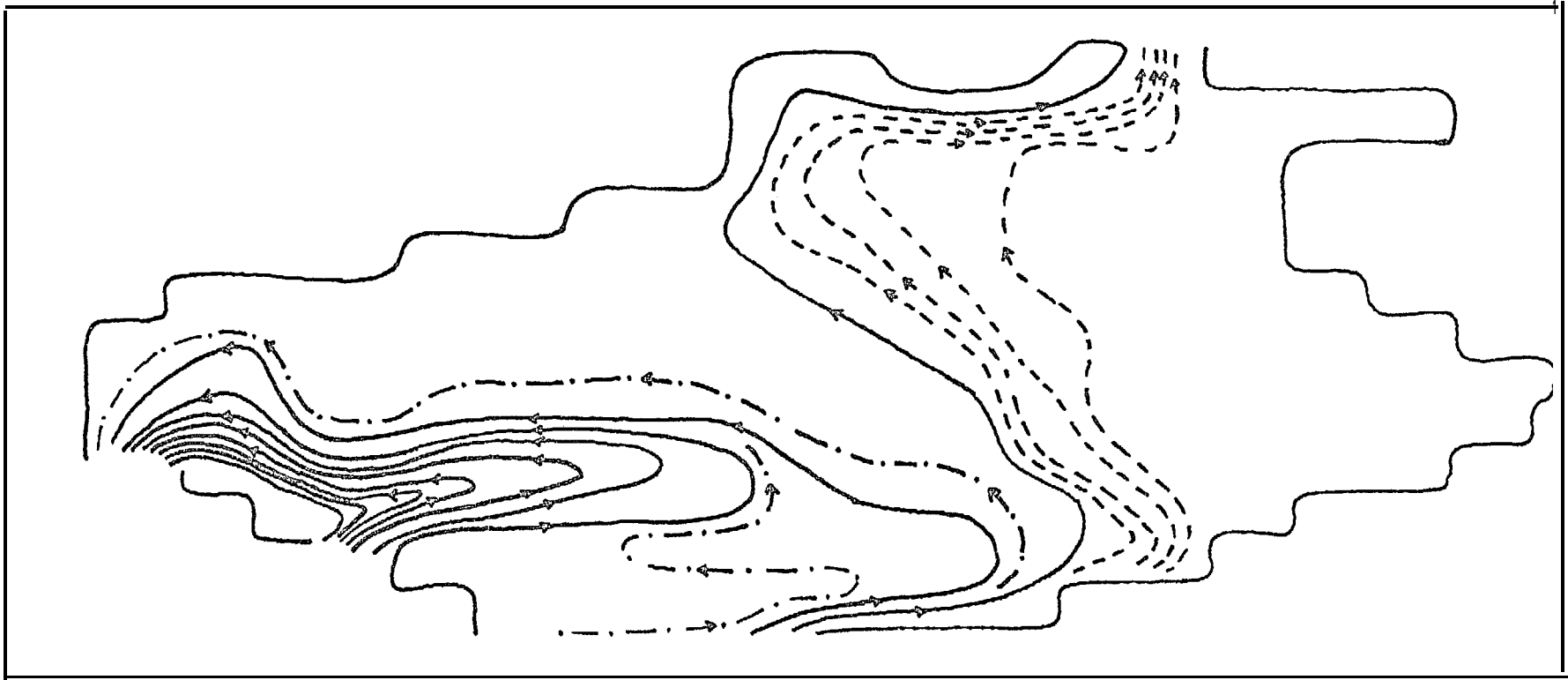


Figure 10. Circulation in the Bering Sea with sources and sinks only.
 Transport Contours - 2.0 Sv ($10^6 \text{ m}^3/\text{sec.}$)
 --- 1.0 Sv
 -.- 0.2 Sv

It is suggested, based on the preliminary analysis above, that a simple model such as this can be valuable for exploring some fundamental physical **processes in the Bering Sea**. On the **other hand**, **it must be recognized that the real ocean is baroclinic, and these** results should be considered only a general guide in an effort to construct the full three-dimensional circulation pattern of the sea.

SECTION VI. STATUS OF COMPUTER

VI-1. Introduction

Graphics output is the most effective means of communicating the results of a numerical model run. The variables are embedded in a multidimensional space, and important features are geometrical or topological properties that must be "seen" to be understood. We have assembled a data processing system intended primarily for the storage and maintenance of graphic information; this system is integrated with other computer systems via telecommunications network links. Hardware development is nearly complete. System software development to fully utilize the equipment will require a minimum of an additional year. Applications software development, in particular an oil spill trajectory model, is underway.

VI-2. Hardware

The graphics system consists of

1. A 40 x 60 inch Tales graphic input tablet for map digitizing,
2. A Tektronix 4051 graphic calculator with tape cassette drive and a joystick.
3. A Tektronix 4662 plotter for hard copy plotting.
4. A DEC PDP-11/34 computer with 64k words of memory (32k currently installed), and 6m byte disk capacity (4m bytes installed).
5. A hard-wired serial communications link to the PMEL PDP-11/55 computer.
6. And a dial-up telephone port.

The peripheral devices all communicate via serial transmission lines. The dial-up telephone port will allow remote execution of a numerical model from any telephone (with suitable terminal equipment).

VI-3. Software

The manufacturer's RSX-11M operating system is used for all data processing functions. The computer is operated in a time-shared multi-programmed mode. This means that a number of programs run simultaneously, sharing resources. Program development, graphics input/output, data preparation, numerical model runs, and remote job operations can proceed at once.

A number of system modifications and extensions are being undertaken to support the particular set of peripheral devices in the system, and the special requirements of the modeling program. Because the applications programs are written under the DEC RSC11-M operating system, they are compatible with the DEC RSX11-D operating system on the PMEL PDP-11/55 with which the modeling computer can communicate via network software over a serial communications channel. The PDP-11/55 has a large disk capacity, magnetic tape drives, and other useful peripherals.

Because graphics is the heart of our man/machine interface, a great deal of attention has been given to providing a rich set of graphics primitives. Improvement, integration, and simplification of these programs will continue to be a major objective.

SECTION VII. REFERENCES

- Danard, 1975: A Numerical Model for Surface Winds in Juan de Fuca, Hare, and Georgia Straits. Report to Atmospheric Environment Services, Downsview, Ontario.
- Lavoie, 1972: "A mesoscale numerical model of lake-affected storms." J. Atmos. Sci. 29_, 1025-1040.
- Lavoie, 1974: "A numerical model of tradewind weather on Oahu". Mon. Wea. Rev. 102, 630-637.
- Reynolds and Walter, 1976: "Nearshore Atmospheric Modification" Annual Report to OCSEAP 1976. Research Unit #347.
- Shuman, 1957: "Numerical Methods in Weather Prediction: II Smoothing and Filtering" Mon. Mea. Rev. _85 357-361.